Aus der Medizinische Klinik und Poliklinik V

Klinik der Ludwigs-Maximilians-Universität München

Director: Prof. Dr. med. Jürgen Behr

Connexin43 gap junction drives fascia matrix mobilization and repair of deep skin wounds

Dissertation

Zum Erwerb des Doktorgrades der Humanbiologie

an der Medizinischen Fakultät der

Ludwig-Maximilians-Universität zu München

Vorgelegt von

Li WAN

aus

Sichuan, China

Jahr

2021

Mit Genehmigung der Medizinischen Fakultät

der Universität München

Berichterstatter:	Prof. Dr. med. Jürgen Behr
Mitberichterstatter:	PD. Dr. med. Gerd Gauglitz
	Prof. Dr. med. Thilo Schenck
Mitbetreuung durch den promovierten Mitarbeiter:	Dr. Yuval Rinkevich
Dekan:	Prof. Dr. med. dent. Reinhard Hickel
Tag der mündlichen Prüfung:	08.07.2021

Table of content

Zusammenfassung

Tiefe und voluminöse Hautwunden werden repariert, indem Fibroblasten und extrazelluläre Matrix aus der Faszie tief unter der Haut austreten und die verletzten Oberflächen mit Narben verschließen. Der molekulare Auslöser dieses neuartigen Reparaturmechanismus ist nur unvollständig verstanden. Hier zeigen wir, dass Cx43 der Schlüssel zur Patch-Reparatur von tiefen Wunden ist. Durch die Kombination von Full-Thickness-Wundmodellen mit Fibroblastenlinien-spezifischen transgenen Linien zeigen wir, dass Cx43 ausschließlich in tiefen Wunden hochreguliert wird, und zwar in spezialisierten Fibroblasten der Faszie tief unter der Haut, die für die Narbenbildung verantwortlich sind. Mit Hilfe von Live-Imaging von Faszienfibroblasten und Fate Tracing der extrazellulären Matrix der Faszien zeigen wir, dass die Hemmung von Cx43 die Oszillationen des Kalziumspiegels in tiefen Faszienfibroblasten unterbricht und dass dies ihre kollektive Wanderung hemmt, die notwendig sind, um die Faszienmatrix in offene Wunden auszuschütten. Cx43 und die Zell-Zell-Kommunikation sind somit Vehikel der Matrixausschüttung und Narbenbildung und notwendig für die Patch-Reparatur von voluminösen Wunden. Diese Erkenntnisse haben weitreichende klinische Implikationen für die Behandlung von Fibrose, überschießender Narbenbildung und gestörter Wundheilung.

Abstract

Deep and voluminous skin wounds are repaired, by outpouring of fibroblasts and extracellular matrix from fascia, deep below the skin, plugging breached surfaces with scars. The molecular trigger of this novel repair mechanism is incompletely understood. Here we reveal that Cx43 is the key to patch repair of deep wounds. By combining full-thickness wound models with fibroblast lineage specific transgenic lines, we show Cx43 is upregulated exclusively in deep wounds, in specialised fibroblasts of the fascia deep beneath the skin that are responsible for scar formation. Using live imaging of fascia fibroblasts and fate tracing of the fascia extracellular matrix, we show that Cx43 inhibition disrupts calcium level oscillations in deep fascia fibroblasts and that this inhibits their collective migrations necessary to outpour fascia matrix into open wounds. Cx43 and cell-cell communication are thus vehicles of matrix outpouring and scar formation, and necessary for patch repair of voluminous wounds. These findings have broad clinical implications for treating fibrosis, aggravated scarring and impaired wound healing.

2 Introduction

2.1 Skin

Skin, the largest and outermost organ in mammals, is highly organized into multiple strata layers, from outer to inner, that include the epidermis, dermis and hypodermis (Kanitakis, 2002). It serves as a protective barrier from the external environment, as well as provides a primary defence against bacterial and viral infections, physical protection from external environmental insults such as dehydration, chemical, mechanical, and UV exposure (Lee et al., 2006). In addition, the skin has further versatile roles in sensation, thermoregulation, metabolic regulation and immune surveillance (Kanitakis, 2002).

2.1.1 Epidermis

The epidermis is the outermost strata layer of the skin, and it is mainly composed of four different cellular lineages. The predominant one are the stratified keratinocytes, which synthesize and secrete the major structural proteins of the stratum corneum (SC). Melanocytes, the second cell type, generate pigment granules, termed melanosomes, containing melanin (Wickett and Visscher, 2006). The third cell type is Langerhans cells, a type of dendritic cells presenting epitope once activated by antigen. Merkel cells is last one, involved in sensation (Moll et al., 2005).

2.1.2 Dermis

The dermis originates from the embryonic mesoderm, and it represents the most abundant connective tissue of the skin. It is composed by two main layers: upper papillary and lower reticular dermis. Both dermal compartments are fundamentally made up of the same fibrillary and connective tissue components namely collagens, which

contributes to the rigidity of the dermis and that supports skin appendages. Approximately 80% of dermal collagen is collagen type I and the remaining belongs to collagen type III and elastin (Epstein and Munderloh, 1978). In addition to connective tissue framework, dermis houses specialised cell types termed fibroblasts, which are the primary cellular source of collagen and elastin (Lynch and Watt, 2018). In addition to fibroblasts, dermis also contains a range of other supportive cells including mast cells, macrophages, lymphocytes and melanocytes, as well as blood vessels and peripheral nerves. The dermis further contains various epidermal appendages that invaginate and reside within the dermis, including sweat glands, apocrine glands, sebaceous glands, hair follicles and nails, which support the functions of the upper epidermal layer. Below the dermis directly is the hypodermis layer, also called subcutaneous layer, which is actually not part of integument system. The hypodermis, consisting areolar and adipose connective tissue, mainly protects the body from damage, provides thermal insulation, and functions as energy reservoir. A layer of striated muscle, below hypodermis known as *Panniculus carnornosus* (PC) muscle, provides skin twitching and contraction functions.

2.1.3 Fascia

Fascia is a gelatinous viscoelastic layer in subcutaneous locations, which implements a frictionless interface between the upper skin and inner rigid structures. The thickness of fascia varies considerable regionally and sexually. For example, murine back skin houses a single layer of fascia underneath muscle and skin. In contrast, several fascia layers, incorporated with adipose tissue, neurovascular and lymphatic tissue, are continuous with skin directly in human without any PC muscle. The fascia underneath the dermis also serves as fat storage, insulator and protection, providing a buffer effect for the underlying muscles, tendons, bones and joints.

2.1.4 Murine skin

Human and murine skin are highly similar in structure and composition. Murine skin is composed of the same layers as human skin, except a far thinner epidermis and hair follicle-populated dermis (Lee et al., 2018; Sougrat et al., 2002).

In mouse skin, hair follicles cycle and transition much more frequently than in human skin (Muller-Rover et al., 2001). In other hand, subcutaneous layers in mouse skin lies directly above a striated muscle layer, the panniculus carnosus muscle, as compared to human skin. Whereas human skin lacks muscle layer, hypodermis is adjacent to fascia layers directly (Dorsett-Martin, 2004). Resident immune cells are apparent similarly present, as both mouse and human skin houses macrophages, mast cells, conventional αβ T cells and a small population of innate lymphoid cells (ILCs). However, the most prevalent immune cells in human skin are Langerhans cells and CD8+ T cells, in contrast with prominent Vγ5+ dendritic and T cells (DETCs) distributing in mouse skin (Pasparakis et al., 2014).

Below is a schematic that summaries the major differences in cell composition and structure between mouse and human skin (Fig. 1.1, 1.2, Table 1.1).
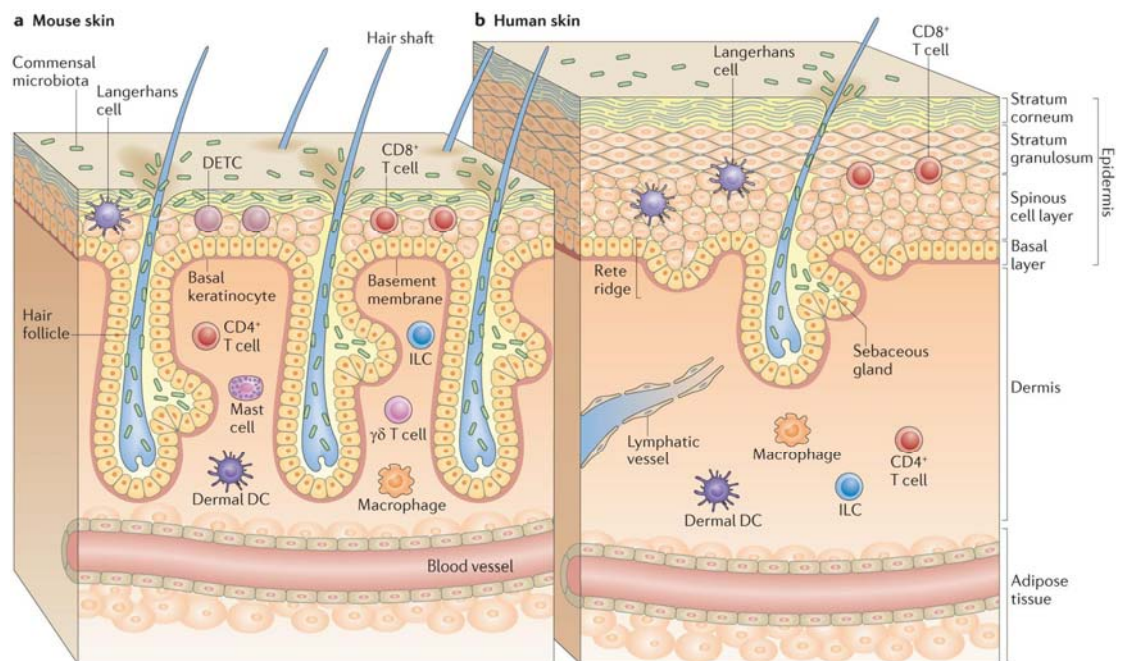
Figure 1.1   Structure of the skin in murine and human. Mouse skin (a) shows

denser hair follicle but thinner epidermis with less cell layers compared with human skin

(b). Several immune cells presented in murine and human skin (Pasparakis et al.,

2014).
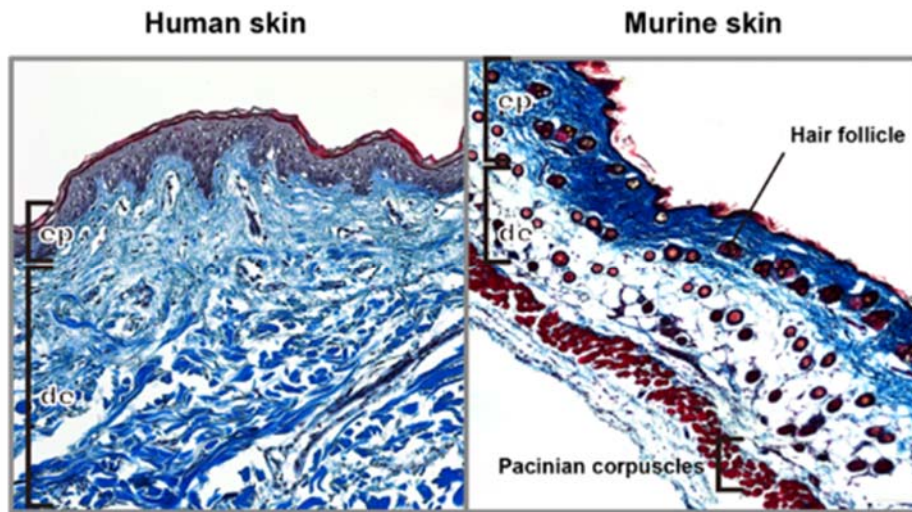
Figure 1.2   Comparative structure of human and murine skin. Trichrome staining of human skin and murine dorsal skin section. **ep** stands epidermis, **de** represents dermis (10x).

Table 1.1   Major differences between mouse and human skin (Wong et al., 2011)

	Mouse	Human
Hair cycle	~ 3 weeks	Regionally, sexual dependent
Epithelial structure	Without rete ridges	Rete ridges
Apocrine sweat glands	Extend from mammary glands	Appeared in axilla, inguinal, and perianal skin regions
Physical properties	Thin, compliant, loose	Thick, relatively stiff, adherent to underlying tissues

Hypodermal thickness	Depends on hair cycle	Fixed
Subcutaneous muscle	Knowns as panniculus carnosus muscle	In neck as platysma
Wound healing	Contraction, fascia patching	Granulation tissue formation, re-epithelization

2.2 Cutaneous wound healing

Intact healthy skin provides protection from outside irritation or injury. Therefore, proper wound healing is an essential physiological process for tissue homeostasis (Karppinen et al., 2019). Generally, skin wound healing is a highly hierarchically orchestrated process involving three overlapping phases. Wound healing initiates with haemostasis, an immune reaction that forms a temporary fibre clot at sites of injury. Haemostasis rapidly stops bleeding and covers the injury site with a provisional fibrin barrier, which deters pathogens and microorganisms within open wounds, amplifies the pro-inflammatory cytokines and immediately consecutive recruiting activated neutrophils into the wound from damaged blood vessels for the next 1 or 3 days, and establishes a first provisional matrix bedding for subsequent stages (Kim et al., 2008). Subsequently within days, the healing process progresses into a proliferative phase, involving fibroblast proliferations in dermis, keratinocyte proliferation in epidermis, and endothelial proliferation that end with angiogenesis. At the same time, wound contraction initiates from the edges of the wound, gradually closing the open skin barrier (Shaw and Martin, 2009). Lastly, fresh matrix is synthesized, deposited within wound, and further remodels over time until maturation, finally, as scar tissue (Dovi et al., 2004; Shaw and Martin, 2009).

2.2.1 Scarring

Over 100 million patients experience skin scarring from burns, surgery, and recreational injury per year, which are a huge burden for both patients and global healthcare systems (Marshall et al., 2018). Scarring is characterized by excess collagen deposition which initiates by specialized fibroblast immigration into wounds (Marshall et al., 2018). Human skin is primarily repaired by scarring. Whereas, superficial skin wounds regenerate as minimal scars, deep and voluminous wounds are physically covered with

dense plugs of connective tissue matrix, called scar tissue (Bayat et al., 2003; Driskell et al., 2013; Gurtner et al., 2008; Rinkevich et al., 2015; Stappenbeck and Miyoshi, 2009; Watts, 1960). However, wound healing in the oral mucosa proceeds rapidly with minimal scar formation compared to back skin injuries (Jiang et al., 2020). Similarly, foetal skin wounds also exhibit highly regeneration ability. Fortunately, stromal cell-derived-factor-1(SDF1) contribute elder to acquire this ability again as wound healing with less scarring (Larson et al., 2010; Nishiguchi et al., 2018).

However, keloids and hypertrophic scars, two fibrotic scars in humans, are usually different from normal mature scars in composition and size, appearing as shiny, hairless, rising above surrounding skin, reaching the reticular dermis. Fibrotic scars are pathological scars that are populated with inflammatory cells and exuberant numbers of fibroblasts, enriched neo-vessels and collagen deposition. So far, Researcher cannot reduce systemic and genetic risk factors though treatments, such as laser treatment, cryotherapy, were developed for keloids and hypertrophic scars (Gauglitz et al., 2011; Ogawa, 2017).

2.2.2 En1 lineage-positive skin fibroblasts

Fibroblasts are the major producers of ECM in both embryonic and adult organs, as well as in tissue fibrosis, and cutaneous scarring (Hinz et al., 2007; Wynn, 2008). Though multiple embryonic lineages of fibroblasts were discovered in the dorsal skin, all scars primarily come from a single fibroblastic lineage, termed as Engrailed-1 (En1) lineage positive fibroblasts (EPFs). EPFs appear as a small subset at early embryogenesis, and expand within the developing skin during embryogenesis. In contrast, En1 lineage negative fibroblasts (ENFs), characterised in the back skin, do not contribute to scar formation. Both fibroblast subsets co-exist in the back skin, where the balance of their

abundance drives the emergence of scar formation during skin development (Jiang et al., 2018; Rinkevich et al., 2015).
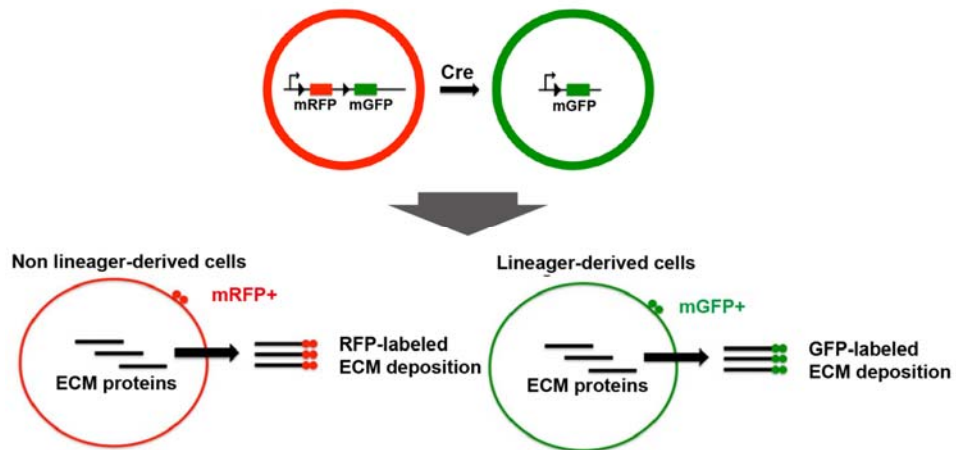
Figure 1.3   Schematic showing differential labeling of connective tissue depending on EPFs and ENFs in mTmG system (Rinkevich et al., 2015).
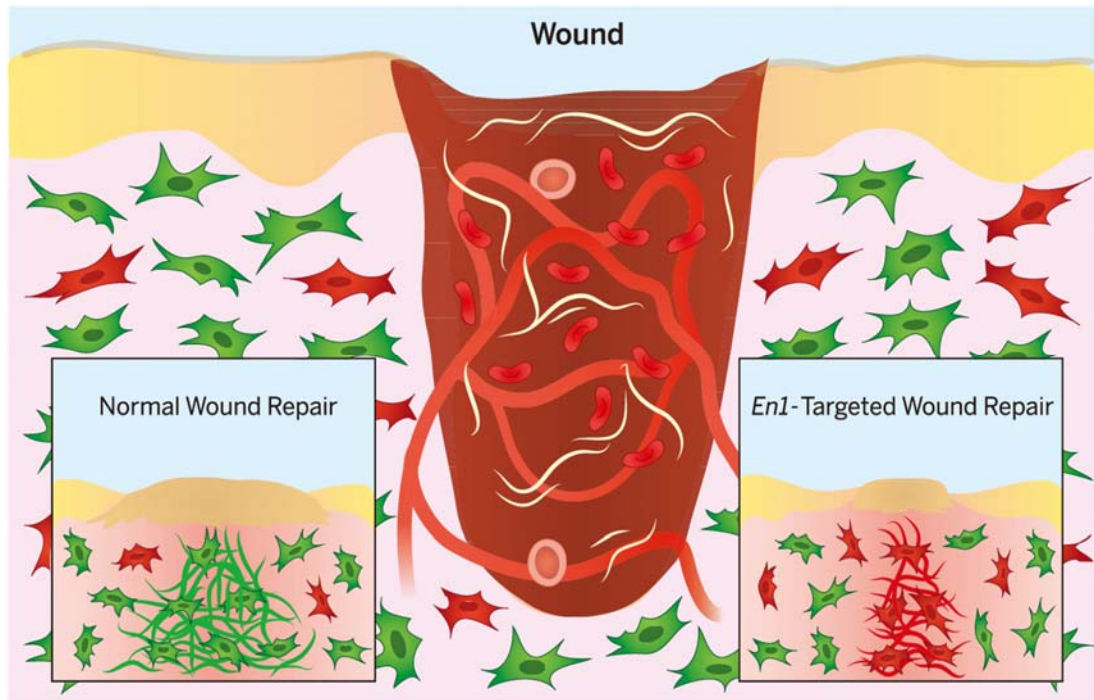
Figure 1.4 EPFs contributing to connective tissue deposition, whereas ablation/ inhibition of En1 fibroblasts reduced scarring (Rinkevich et al., 2015).

2.2.3 EPF in superficial fascia

Superficial fascia, in murine back skin, is a connective tissue that is separated by panniculus carnosus muscle, whereas, fascia in humans is much thicker and incorporates fibroblasts, vascular and matrix. Studies discovered that subcutaneous fascia largely took part in provisional scar tissue and reduced wound size. En1 lineage fibroblasts appear to be the major fascia fibroblasts contributing to scar. Fascia fibroblasts expand in skin surface after wounding, and trigger surrounding extracellular jelly-like matrix moving into wound (Correa-Gallegos et al., 2019). However, it is still unclear how fascia EPFs, but not dermal or oral mucosa fibroblasts, cause scarring after wound.
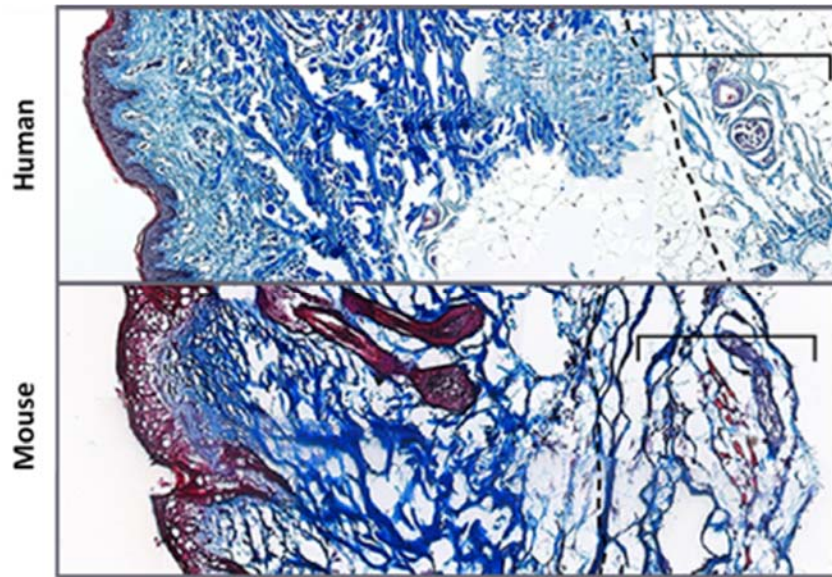
Figure 1.5   **Fascia in human and mouse skin.** Line separates fascia and dermis.
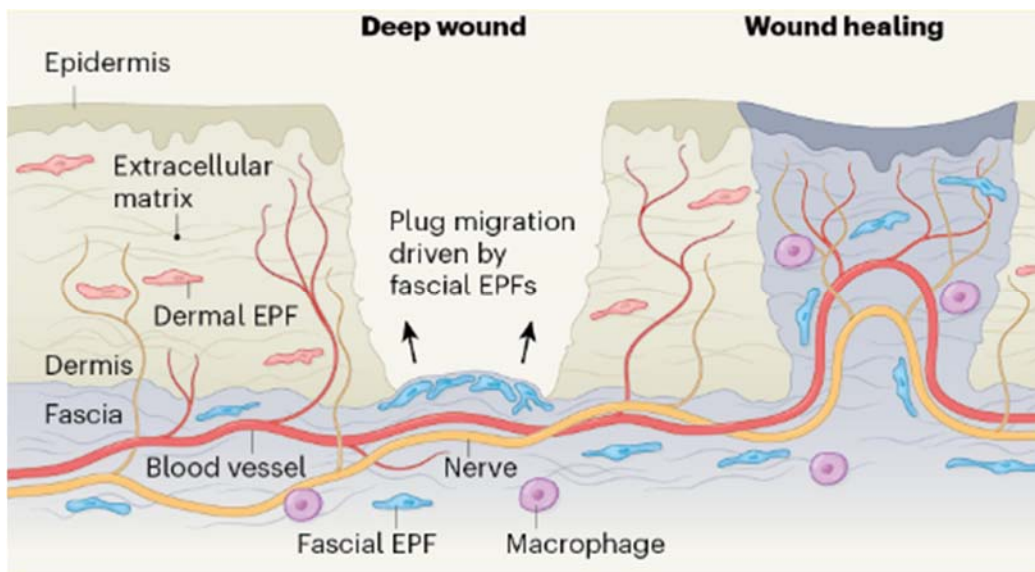
Figure 1.6   **Process of deep skin wounds healing.** Fascia, containing EPFs, ECM,

blood vessels, macrophages and nerve, penetrates into skin and seals the wound.

(Coles and Buckley, 2019).

2.2.4 ECM on scar formation

ECM, is a dynamic scaffold composed of water, proteins and polysaccharides. It undergoes active remodeling and rearranging during development as well as during organ morphogenesis. Overproduction of ECM, especially in scar formation, causes pathological scarring and load a larger burden for internal organs (Coentro et al., 2018; Karppinen et al., 2019). Interestingly, cultured dermal fibroblasts could steer ECM movement or remove individual fibronectin fibers and collagen *in vitro*. In addition, matrix movements occurring during injury quickly seal large open wounds, and inversely, blocking EPFs migrations inhibits scar formation (Correa-Gallegos et al., 2019; Kurpios et al., 2008; Tseng Q, 2012).
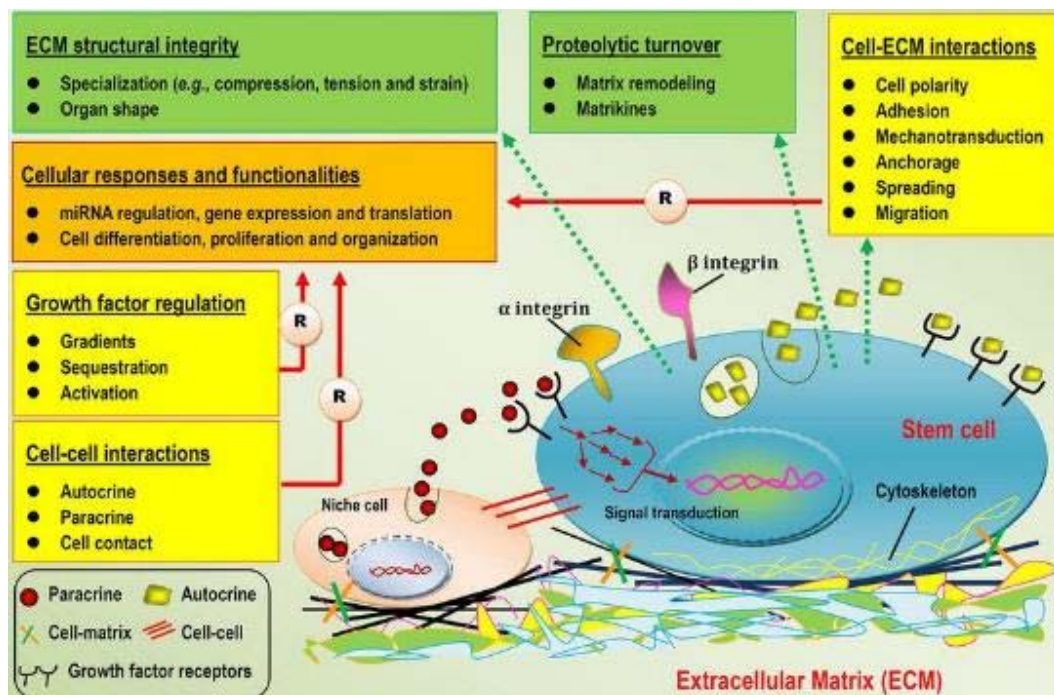
Figure 1.7   Extracellular matrix (ECM) functions and cross talking at the cell–cell and cell–matrix interfaces (Chen and Liu, 2016).

2.3 Gap junction

Mammalian gap junctions are communication channels that stitch adjacent cells (Tarzemany et al., 2017). Six connexin (Cx) subunits of gap junction, merge together coupling cytoplasmic and permitting intercellular passage of ions and small molecules such as Ca^{2+}, ATP and cAMP (Chen et al., 2016; Wong et al., 2016). Cx43, one of the major Connexin in mammalian skin, is a ubiquitous gap junction targeting wound healing responses (Wong et al., 2016). For example, Cx43 deficiency and downregulation accelerated wound closure in mice, and attenuated diabetic wounds in rat model (Becker et al., 2012; Cogliati et al., 2015; Qiu et al., 2003). The oligo peptide inhibiting Cx43 is also currently under Phase III clinical trial for treating diabetic foot ulcers (Montgomery et al., 2018). However, the direct functions of Cx43 *in vivo*, especially in fascia and deep skin wounds remain unknown. As connexin-based therapeutics are being further explored pre-clinically in injury of organ, identifying repair mechanism allow the development of improved, targeted therapies and elucidation of universal repair mechanisms.
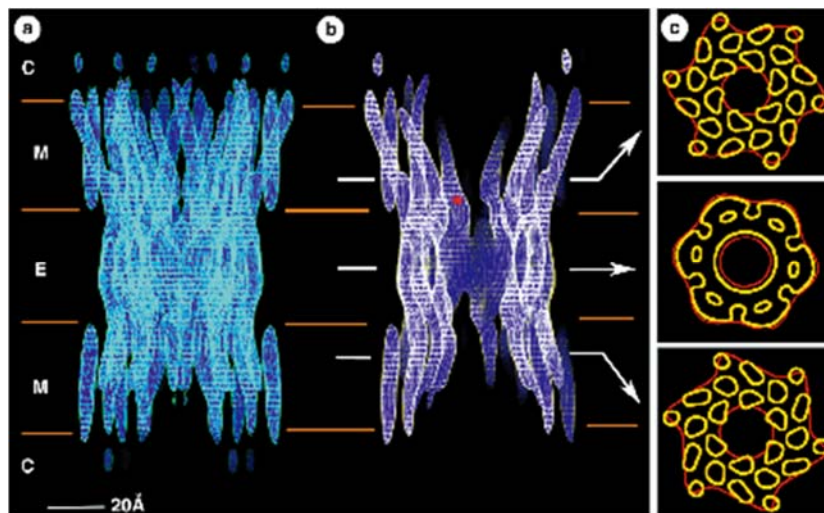
Figure 1.8   3D map of recombinant gap junction. (a and b) showed the side view and density of gap junction. (c) Transverse view of gap junction at position indicated by

white arrows. Letter C represents cytoplasmic space, M is membrane bilayers, E means extracellular gap (Unger et al., 1999).

Gap junction, encoded by connexin gene in both vertebrates and invertebrates, classifies three types, known as α, β and γ, responding to conserved protein motifs (Harris, 2001). All connexins present highly specialized transmembrane structures, linking double tandem extracellular loops with triple cysteine residues forming disulfide bonds such as CX6CX3C in one extracellular terminus and CX4CX5C in the other extracellular terminus, and similar topology according to their structure, especially in humans and mice (Krutovskikh and Yamasaki, 2000). However, the structure of C-terminus, for example, in connexin 43 (Cx43), is randomly coiled with two helical structures. It interacts with various protein partners, including ZO-1, cadherin, catenin, tubulin and microtubules (Sorgen et al., 2004). Residues 228~260 of Cx43 directly interact with tubulin and microtubules, and regulate permeability of Cx43 by

phosphorylation and signal transduction regulated by TGF-β pathway (Saidi Brikci-Nigassa et al., 2012).
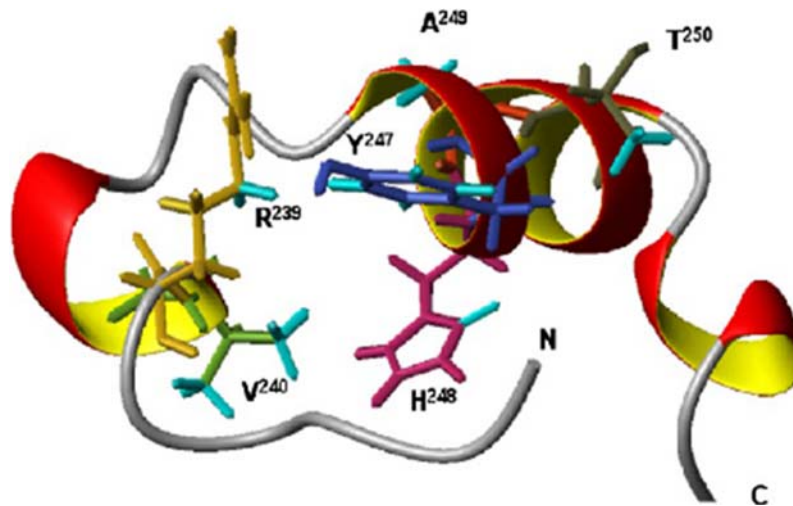
Figure 1.9   **The C-terminus Cx43 binding with tubulin.** The binding negatively regulated by phosphorylation Y247, a target for Src kinase (Saidi Brikci-Nigassa et al., 2012).

Genomic study revealed that connexin ubiquitously expressed on all vertebrates, most of them clustering together within chromosomes 1 and 13 in human. However, more than 20 connexins are named into three subfamilies α, β and γ in humans (Nielsen et al., 2012). Almost all cells express at least one kind of connexins due to gene diversity, for example Cx26, Cx30, Cx43 has been found in keratinocytes, while in Schwann cells is Cx30.2 and Cx32 (Lin et al., 2003; Zhang and Cui, 2017). Those mostly similarity imply that the connexin are likely derived from one gene duplication events.
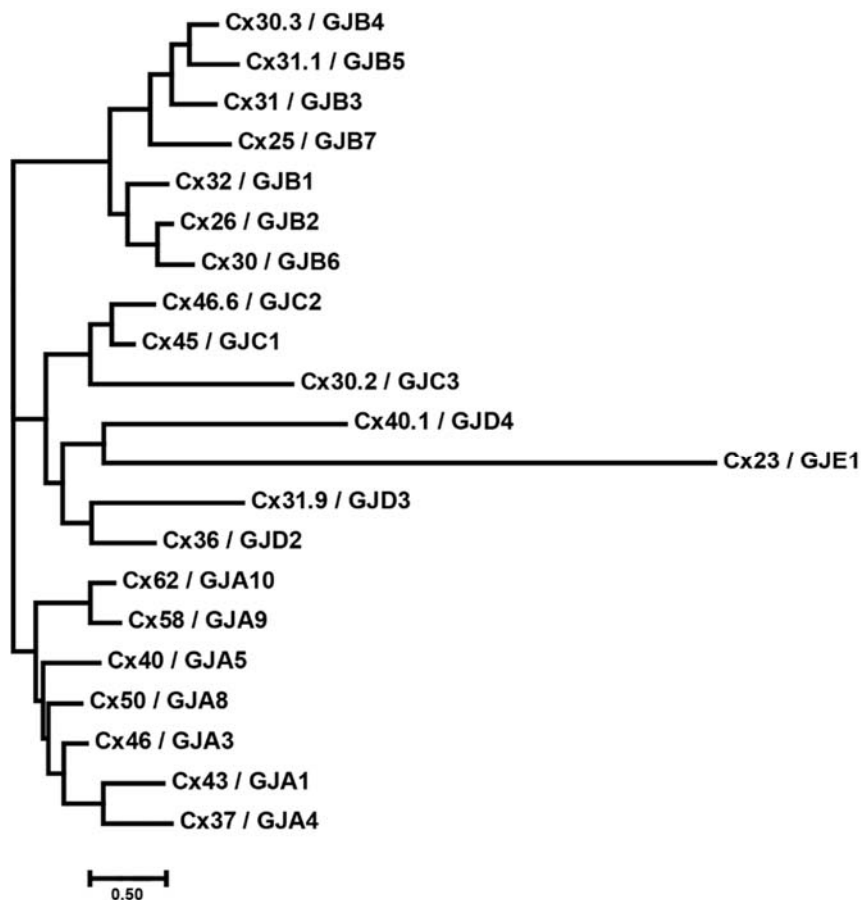
Figure 1.10   All connexins family from human alignment. More than 20 connexins are classified into three subfamilies α, β and γ in humans.

2.3.1 Gap junction in wound healing

Gap junction play important roles in cell-cell communication, cell morphology and polarity, and influence the adhesiveness of cells and directionality of cell migration (Wright et al., 2009). However, abnormal connexin expression was associated with dysregulated cell proliferation, migration and wound healing rates. Cx43, stabilizing a series of proteins, including CDH2 and ZO-1, are required for cell-to-cell adhesion and cell migration. Consecutive high levels of Cx43 in diabetic wounds significantly ameliorating the process of healing was observed in diabetic skin (Wright et al., 2012).

Alternatively, as the C-terminus of Cx43 is known to interact with cytoskeletal components or with P120ctn/ Rho GTPase, downregulation of Cx43 could redirect the motility of keratinocytes at the wound edge, spurring them to migrate and close the wound, which underlie Cx43 has potential tremendous therapeutic value (Derangeon et al., 2008). Blocking Cx43 by antisense peptide accelerated the wound closure and granulation tissue formation and reduced scar size after burn injury, which was beneficial effect in rat model diabetic ulcer (Nakano et al., 2008; Wong et al., 2016). Hence, competing inhibitory peptide of Cx43 in intracellular signalling, currently, is under clinical trial of Phase III for curing diabetic foot ulcers (Montgomery et al., 2018; Zhang and Cui, 2017). On the other side, increased Cx43 expression was induced by TGF-β1, which promotes scar formation via Erk/ MMP-1/ Collagen III pathway (Li et al., 2019). Further reports illustrated that the sustained inhibition of Cx43 accelerated efficient wound healing, and altered mesenchymal cell movement patterns and feather bud elongation in chicken dorsal skin explants (Li et al., 2018).

2.3.2 Gap junction targeting therapy

Mimetic peptides, identical to defining sequences of connexin lying in the N-terminus, extracellular loops and transmembrane domains, are more specific targeting connexin. The popular peptide, Gap 27, possessing sequence homology of various connexin subtypes, has been frequently employed to inhibit intercellular communication in various inflammatory diseases (Elbadawy et al., 2016). Indirectly inferring from arterial contractility studies, the IC50 of Gap27 is 20-30 μM whereas higher concentration, at 200-300 μM, may block other channels, like Pannexin-1 (Glass et al., 2015). In parallel with a reduction of Cx43 phosphorylation, gap junction also mediates apoptotic cell death or increases sensitivity to pro-apoptotic agents (Lin et al., 2003). Although the

therapeutic potential of connexin is undeniable, more effort should be taken into studying the regulation and functions of these proteins.

2.3.3 Calcium signalling

Organ development and tissue regeneration require extensive coordination among heterogeneous cell populations to generate complex organ morphologies (Brodskiy and Zartman, 2018). Ca^{2+}, a ubiquitous intracellular signalling molecule responds to diverse stimuli and participates in various physiological processes, such as cell proliferation, differentiation, apoptosis and migration (Brodskiy and Zartman, 2018). When concentrating on wound healing in multi-layered skin, a rapid influx of calcium, firstly, comes around the wound; then a short-lived ranged wave spreads through healthy neighbouring cells. Moreover, the larger the wound injured, the faster the wave spreading, in which calcium waves pass through adjacent cells suggesting that gap junctions and calcium ions make up signalling bridges. Furthermore, X-ray crystal structures of the human Cx26 gap junction channel with and without bound Ca^{2+} has been described.(Bennett et al., 2016). Due to T- and L- type Ca^{2+} channels involving cellular and organ functions, Ca^{2+} channel blockers, e.g., efonidipine which disrupts the Ca^{2+} oscillations by selective inhibition of both T- and L-type channels, are pivotal to the synthetic function of human pulmonary fibroblasts, which have been used in clinical practice (Mukherjee et al., 2013). Furthermore, rapid, transient increases in intracellular calcium have been reported in scratch wounds and single-cell wound assays (McNeil and Steinhardt, 2003; Nakano et al., 2008). Induced Ca^{2+} oscillations also enhanced feather bud elongation in chicken (Li et al., 2018). In Summary, calcium has long been a candidate for discovering the earliest signal during wound repair. Understanding mechanisms under the wound healing process with personalized condition would pave a

road for developing pharmacological tools to slow down or even to speed up normal wound healing.
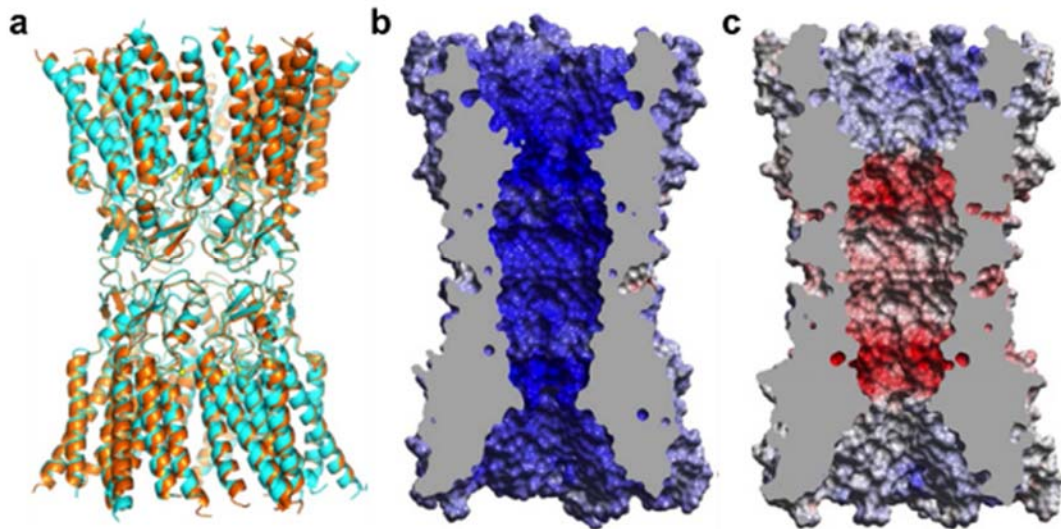
Figure 1.11   Gap junction bound with calcium. (a) The calcium-bound (orange) and calcium-free (cyan) gap junction are almost identical. (b, c) depicted gap junction electrostatic surfaces, in which calcium binding (b) establishes a positive surface potential in the pore (blue) that limits molecular permeation (Bennett et al., 2016)

3 Hypothesis of the study

Deep and voluminous skin wounds are repaired by plugging breached surfaces with scars. The molecular mechanism steering fibroblast and ECM from fascia into scars is incompletely uncovered. The hypothesis was that Cx43, cell-cell communication junction, are vehicles of matrix outpouring and scar formation, and necessary for patch voluminous wounds.

To reveal the Cx43 role in deep wounds healing, full-thickness wound models in specific fibroblast lineage transgenic mouse lines, and fate tracing of the fascia extracellular matrix were applied.

5 Materials and methods

5.1 Human samples

Fresh human skin and keloid biopsies were collected by the department of Dermatology and Allergology, Klinikum rechts der Isar, Technical University Munich (reference number 85/ 18S). Informed consent was obtained from all subjects prior to skin biopsies. Upon collection, these samples were directly processed with PFA fixation and then OCT embedding followed by histological or immunofluorescent analyses.

5.2 Mice strains

All Mouse strains (C57BL/6J, En1^{Cre}, R26^{mTmG}, R26$^{LSL-H2B-mCherry}$, R26$^{VT2/ GK3}$, Rag2$^{-/-}$) were obtained from Jackson laboratories or generated at the Stanford University Research Animal Facility as described previously (Rinkevich et al., 2015). En1^{cre} transgenic mice were crossed with R26^{mTmG} two-color membrane reporter mice or R26$^{LSL-H2B-mCherry}$ nuclear reporter mice. All mice were bred and maintained at the animal facility of Helmholtz Centre Munich. All animal experiments were approved by the Government of Upper Bavaria and registered under the project 55.2-1-54-2532-61-2016 and conducted under strict governmental and international guidelines. This study is compliant with all relevant ethical regulations regarding animal research.

5.3 Genotyping

Cre-positive (Cre^{+}) was identified by detecting relevant fluorescence of the dorsal dermis under microscope. Genotype of Cre^{+} inserted with a 200-base pair fragment (Cre$^{+/-}$) was performed by PCR to distinguish from the wildtypes (Cre$^{-/-}$). Briefly, genomic

DNA from the ear clips was extracted using Quick Extract DNA extraction solution (Epicenter) following the manufacturer's guidelines. Then 1 µL DNA extract was added to 24 µL Qiagen PCR reaction mixture containing forward primer "Cre_genotype_4F"- 5´ ATT GCT GTC ACT TGG TCG TGG C- 3´ (Sigma) and reverse primer "Cre_genotype_4R"- 5´ GGA AAA TGC TTC TGT CCG TTT GC- 3´ (Sigma). PCR reactions were initiated into denaturation for 10 min at 94 °C, amplification for 30 cycles: denaturation for 30 s at 94 °C, hybridization for 30 s at 56 °C, elongation for 30 s at 72 °C and final elongation for 8 min at 72 °C then cooled to 4 °C. Reactions were analysed by gel electrophoresis.

The 2% agarose gel was prepared by mixing 2 mL of 50x TAE buffer, 2 g agarose in 100 mL ddH$_2$O and heating with microwave to melt completely. To stain DNA fragments in gel, 5 µL SYBR Green Master Mix was added once the solution was cooled to rough 60 °C. The gel was filled into a mould with the fitted comb and allowed to cool down at room temperature. Once the gel solidified, it was placed in a tank with the TAE buffer. A DNA ladder was loaded in the first lane and 15 µL sample reaction solution in the rest wells. Then electrophoresis was run at constant voltage 120 for 12 min. Finally, gel was visualized on a UV trans-illuminator and photographs were taken on a digitall camera (UVP Bioimaging Systems).

5.4 Skin-fascia explants assay

Dorsal skin was harvested from new-born (postnatal day 0-1) C57BL/6J or En1^{cre};R26^{mTmG} mice or nuclear reporter En1^{Cre};R26$^{LSL-H2B-mCherry}$ mice and washed with HBSS. Full-thickness round skin pieces were taken with 2 mm biopsy punches (Stiefel) and cultured in 200 µL DMEM/F-12 (Thermo Fisher) medium containing 10% FBS (Life technologies), 1% GlutaMax (Thermo Fisher), 1% Penicillin/streptomycin (Thermo

Fisher) and 1% MEM non-essential amino acids (Thermo Fisher) in 96-well plates in a humidified 37 °C, 5% CO_2 incubator. In addition, the skin pieces were cultured submerged in medium with dermal side face up.

Medium was routinely replaced every other day stimulated with 10 ng/mL TGF-β 1, 2 µM SB 431542, 1 µg/mL 2-APB, 8 µM GAP 27 separately. On day 3 or day 5 of culture, samples were washed by PBS and fixed with 2% PFA overnight at 4 °C. After fixation, the tissue were processed for whole-mount bright field imaging or whole-mount fluorescent staining directly or embedded in OCT following with 6 µm cryosections for trichrome staining or immunofluorescence staining.

5.5 Excisional wounds on mice

The 8-10 weeks old En1^{cre};R26^{mTmG} mice were anesthetized with medetomidine at 500 µg/kg, midazolam at 5mg/kg and fentanyl at 50 µg/kg (MMF) body weight. Two full-thickness excisional wounds were created with a 5 mm diameter biology punch (Stiefel) under supply with analgesia. Wounds were harvested at day 0, 3, day 5, day 7 post-surgery by cutting out and washing with PBS, following fixation with 2% PFA immediately at 4 °C overnight. After washing 3 times with PBS, wounds were sliced into two half parts in the middle and then embedded in OCT and processed for histology staining.

5.6 Splinted wounds on mice

Splinting rings with outer diameter 12 mm and inner diameter 6 mm were made of 0.5 mm silicone sheet (Grace Bio-Labs, CWs-0.5), and sterilized with 70% ethanol for 30 min followed by washing with PBS. Air dried rings were kept in a sterile bottle until surgery. Before operation, mice were anesthetized with MMF. Dorsal hair was removed

by incubating skin with hair removal cream for 5 min. Two full-thickness excisional wounds on back skin were created with a 5 mm diameter biology punch (Stiefe). To prevent skin contraction around wounds and allow the wound to close by re-epithelialization and granulation tissue formation, silicone rings with one side applied with silicone elastomer super glue (KwiK-Sil Adhesive) were sutured onto the excisional wounds. Mice were supplied with analgesia after surgery. Mice were subcutaneously injected with 60 µL 2-APB at 4 µg/mL or 60 µL GAP27 at 80 µM or 60 µL Nifedipine at 10 µM, 60 µL 0.1% DMSO or saline on every second day for each group. After 21 days, the hair follicle of the back skin was shaved followed by hair removal cream. Then scars were dissected and washed with PBS, following fixation with 2% PFA immediately in 4 °C overnight. After washing 3 times with PBS, wounds were sliced into two parts in the middle and then embedded in OCT.

5.7 Masson's trichrome staining

Skin-fascia explants tissues were fixed with 2% PFA at 4 °C overnight, and washed three times with PBS. Whole mount bright-field images were taken with a Leica M50 stereo microscope equipped with a Leica DFC310 FX camera (Leica). Subsequently, tissues were embedded in OCT (Sakura Finetek) and subjected to slice in 6 µm cryosections with Hyrax C50 Cryostat (Zeiss).

Masson's trichrome staining was performed using a Masson's trichrome staining kit (Sigma-Aldrich HT15) according to manufacturer instructions. Briefly, cryosections fixed in cold acetone in minus 20 °C for 5 min, and then air dry for 5 min. After wetting slides in deionized water for 2 min, sections were incubated in preheated Bouin's solution (Sigma-Aldrich HT10132) at 56 °C for 15 min. Then wash in cold tap water to remove yellow color from sections, the sections were stained with Weigert's Iron Hematoxylin

(Sigma-Aldrich HT1079) at working concentration for 5 min. Thereafter, the sections were treated with Massion's trichrome stain kit (Sigma-Aldrich HT15) by sequentially incubating at room temperature in Biebrich scarlet-acid fuchsin solution for 5 min, working concentration of Phosphotungstic / Phosphomolybdic acid (HT152-250ML/ HT153-250ML) for 5 min, aniline blue solution for 10 min, and 1% acetic acid for 2 min. After dehydration in 80% ethanol, 100% ethanol I, 100% ethanol II consecutively for 5 min separately, the sections were cleared with Roti-Histol (Roth 6640) and mounted with a Roti-HistoKit (Roth 6638). In white field, collagen was stained blue, cells in red and nuclear in black. For the quantification of scar areas, trichrome images were converted to CMYK and the cyan channel was assigned to quantify blue-stained collagens.

5.8 Immunostaining

For immunostaining, sections were rinsed with PBS for three times and then incubated with 5% BSA in PBS for one hour at room temperature to block the non-specific binding of antibodies. Then sections were incubated with the primary antibodies rabbit anti-Cx43 (Sigma-Aldrich C6219, 1:200), goat anti-CD 26 (Sigma-Aldrich, 1:200) or rabbit anti-collagen I (Rockland 600-401-103-0.5, 1:150) or goat anti-CD 26 (Sigma-Aldrich, 1:200), Goat anti α-SMA (Abcam, ab21027, 1:200) or Rat anti F4/80 (Abcam, ab90247, 1:200) in 2% BSA at 4 °C overnight. Sections were washed with PBS for three times and incubated with the AlexaFluor 594-, or AlexaFluor 647-conjugated secondary antibodies (Life technologies, 1:500) against the relevant species for 1 hour at room temperature. Next, sections were washed three times in PBS and finally mounted with fluorescent mounting media with DAPI (Fluoromount-G, Thermo Fisher scientific 00-4958-02). Photomicrographs were taken with a Zeiss AxioImager microscope with ZEN blue software (Carl Zeiss).

5.9   3D imaging for murine skin

Fixed skin-fascia explants from En1[cre];R26[mTmG] mice were pre-incubated with PBS, containing 0.01% Thimerosal (Sigma T8784), 0.5% Triton-X100 (Sigma X100) and 0.2% gelatin (Sigma G1393), termed as PBS-GT, at room temperature for 18 h. Then samples were incubated with the primary antibodies anti-43 (Sigma-Aldrich, C6219, 1:100) in PBS-GT at room temperature for 24 h. After washing in PBS-GT, samples were incubated in Alexa Fluor 647-conjugated goat anti-rabbit IgG (Thermo Fisher Scientific, 1:250) in PBS-GT at RT for 24 h. After incubation, samples were washed with PBS-GT. Finally, samples were embedded into 2% NuSieve GTG agarose (Lonza 859081) in a 35 mm dish (Falcon 351008). Whole-mount fluorescence 3D imaging was performed under a Leica SP8 MP (Leica, Germany). Tiles were merged by using the Leica Application Suite X (v4.8, Leica) with smoothing overlay blending. Then data were visualized with Imaris software (v9.1.0, Bitplane, UK) under contrast and brightness optimisation.

5.10 Dermal EPFs purification

Back skin from En1[cre]; R26[mTmG] adult mice were harvested and minced with surgical scissors. The tiny pieces were digested with an enzymatic cocktail containing 1 mg/mL of collagenase IV, 0.5 mg/mL of Hyaluronidase, and 25 U/mL of DNase I in HBSS (Thermo Fisher Scientific), and incubated in 37 °C water bath for 30 min. DMEM containing 10% FBS was added to stop the enzymatic reaction. The suspension was filtered through a 40 µm cell strainer. After washing, the pellets were incubated with APC-conjugated lineage maker anti-mouse CD31 (PECAM-1), CD45, Ter119, Tie2 (CD202b) or EpCam (CD326) (BioLegend) and eFluor660- conjugated anti-mouse Lyve-1 (Thermo Fisher) on ice in dark for 30 min. Subsequently, cells were resuspended in FACs buffer with sytox blue dye (Thermo Fisher Scientific) for dead cell exclusion. Finally, cells were sorted on a BD

FACSAria III with 100 μm nozzle. The viable (Sytox blue), lineage-negative cells (Lin⁻: CD31⁻, CD45⁻, Ter119⁻, Tie2⁻, EpCam⁻, Lyve-1) were sorted into ENFs (Lin⁻RFP⁺GFP⁻) and EPFs (Lin⁻RFP⁻GFP⁺) based on RFP and GFP fluorescence.

Collected cells were seeded on the 8 well chamber (ibidi) with DMEM/F-12 medium containing 10% FBS, 1% GlutaMax (Thermo Fisher), 1% Penicillin/streptomycin (Thermo Fisher) and 1% MEM non-essential amino acids (Thermo Fisher), and incubated in humidified 37 °C, 5% CO_2 incubator. Every other day, the media in the chamber was replaced by gently pipetting out the old media and replacing it with pre-warmed fresh media. Once the cells became 60% - 70% confluent on the bottom of the chamber, EPFs were stimulated with 10 ng/mL TGF-β 1, or 2 μM SB 431542, 1 μg/mL 2-APB, 8 μM GAP 27 separately for 24 h.

5.11 Live imaging of cells migration

Full-thickness back skin biopsy collected from En1^Cre; R26^LSL-H2B-mCherry newborn embryos were cultured for 4 days. Then sample were embedded in 4% agarose (Lonza, 859081) in a 35 mm dish (Corning, 351008). Then samples were submerged in imaging medium phenol-red free DMEM/F-12 (Thermo Fisher Scientific, 21041025) containing 10% KnockOut Serum Replacement (Thermo Fisher Scientific, A3181501), 1% GlutaMAX (Thermo Fisher Scientific, 35050038), 1% Penicillin/streptomycin (Thermo Fisher Scientific, 15140122), and 1% MEM non-essential amino acids (Thermo Fisher Scientific, 11140035). Time-lapse imaging was performed with Leica SP8 MP (Leica, Germany) under a modified heating and gas control incubation system (ibidi 10915 & 1192) with

37 °C and 5% CO_2 during imaging. Z-stacks images were recorded every 15 minutes for 12 h.

5.12 Cell tracking analysis

Cell tracking of Skin-fascia explants from En1[Cre];R26[LSL-H2B-mCherry] mice was performed under Imaris software package (v9.1.0, Bitplane, UK). Tracks were generated using the fluorescence intensity-based detection tool. Particles represents the nuclei of Cre-positive cells were filtered out. Tracks were visualized as a line indicated in the image.

5.13 Dye transfer assay in fibroblasts

NIH 3T3 fibroblasts (ATCC) were cultured in DMEM/F-12 medium containing 10% FBS (Life technologies), 1% GlutaMax (Thermo Fisher), 1% Penicillin/streptomycin (Thermo Fisher) and 1% MEM non-essential amino acids (Thermo Fisher). Culture medium was replaced every other day. Monolayer of 3T3 cells at 70% confluence was labelled with 2.5 ug/mL calcein-AM (Invitrogen) at 37 °C for 30 min. After dissociation with 0.25% trypsin-EDTA (Gibco), labelled cells were mixed with unlabelled cells at a ratio of 1:10. One hour time-lapse imaging was performed every 5 min using Zeiss Observer Z1 (Zeiss, Germany). During capturing, ambient temperature was set to 37 °C with 5% CO_2-supplemented air.

5.14 Time-lapse Ca^{2+} imaging in fibroblasts

NIH 3T3 cells were cultured in an 8-well glass chamber (ibidi). The mixture of 4 µM AM-Fluo-4 Ca^{2+} dyes (Invitrogen) and 0.04% pluronic F-127 (Sigma) were loaded on cells for 25 min in a 37 °C with 5% CO_2-supplemented incubator. After washing with PBS, 20 min time-lapse imaging was performed every 5 s using Zeiss Observer Z1 (Zeiss, Germany)

at 37 °C with 5% CO_2-supplemented air. Labelled calcium indicators are shiny once Ca^{2+} binding. Cell signal tracking was processed with ImageJ (version 1.52 e).

5.15 Chimeric skin transplantations

Full-thickness with 6 mm-diameter biopsies were collected from the back skin from $R26^{mTmG}$, $R26^{VT2/GK3}$ adult mice. At the bench, the fascia together with muscle layer was carefully separated from the dermis and epidermis using forceps and a 26G needle under a fluorescent stereomicroscope (Leica). Chimeras were stacked by placing the epidermis+dermis portion of a mouse strain on top of the muscle+fascia of another strain and leave it in a 35 mm culture dish with 2 mL of DMEM/F12 at 4 °C for 20 min. Then, a 2 mm "deep" full-thickness was excised from the chimeric graft using a biopsy punch in the middle of the biopsy. To create "superficial" wounds, the 2 mm excision was operated only in the epidermis+dermis, prior to reconstitution with the bottom part. "Wounded" chimeric grafts were then transplanted into freshly-made 5 mm-diameter full-thickness excisional wounds on the back of either $RAG2^{-/-}$ or Fox Chase SCID immunodeficient mice. To prevent graft moving, a transparent dressing (Tegaderm, 3M) was placed on the top after the graft drying for 20 minutes. Mice received subcutaneous injection of saline or 80 uM GAP 27 every other day after post-wounding. Wounds samples were collected by 8 mm punch at 14 days post-wounding and processed for cryosection and imaging by fluorescence microscopy. To increase the success rate of transplantation, emptying host blood from the fresh wound before the transplant and leaving the graft dry at least 20 min before ending the anaesthesia should be executed carefully.

5.16 In situ matrix tracing experiment

To label matrix subcutaneously, 8-10 weeks C57BL6/J mice received 20 µL FITC NHS ester at 10 mg/mL in physiological saline with 0.1 M sodium bicarbonate pH 9 (Life technologies, 46409) on four and two days before wounding. Full thickness excisional wounds in 5 mm were created along the labelled area. Subsequently 60 µL saline or GAP 27 at 80 µM was subcutaneously injected around the wounds on every other day. Wounds were harvested on day 7 post-wounding, and fixed in 2% PFA at 4 °C overnight. After washing with PBS, tissue was embedded in OCT and subjected to cryosections.

5.17 Image analysis and statistic

Images were processed and analysed with ImageJ (version 1. 52e). For measuring scar area, a brush tool was used to mask scar area. Calcein-AM and calcium Fluo-4 AM signal in time-lapse images were tracked post subtracting background.

Statistical analyses were performed with GraphPad Prism (v8.0). Statistical significance was assessed by Student's t-test to compare two groups or one-way ANOVA with Tukey's multiple comparisons. All results are represented as mean ± SEM. The exact numbers N and p values are depicted in the figure legends.

Table 3.1   Components of the quantitative qPCR master mix

Mastermix component	Volume per Reaction
Coral Buffer	2.5 µL
dNTPs	0.5µL
Taq polymerase	0.125 µL

Water	19.875 μL
DNA	1μL
F-Primer	0.5μL
R-Primer	0.5 μL
Total	25 μL

Table 3.2   Main chemicals and reagents

Chemicals and reagents	Source	Identifier
2-Aminoethyldiphenylborinate (2-APB)	Sigma-Aldrich	D9754-5G
GAP 27	Sigma-Aldrich	G1794-2MG
Recombinant murine TGF-β1	R and D Systems	7666-MB-005
TGF-β RI Kinase Inhibitor VI (SB 431542)	Merck Millipore	616461-5MG
Nifedipine	Sigma	N7634-1G
Calcein-AM	LIFE Technologies	C1430
Fluo-4, AM	Life technologies	F14201

7 Results

7.1 Injury induces gap junction formation in fascia fibroblasts

7.1.1 Expression pattern of Cx43 on human normal skin and keloid

To investigate whether fibrosis involved with Cx43 in skin wounds, human normal skin and keloid scars were collected and performed histological staining. When looking into Cx43 expression in human keloid scars compared to normal skin, the immunostaining showed that Cx43 was scarcely expressed in the dermis of normal skin, but overwhelmingly abundant in keloid scars, with near uniform expression (**Fig. 4.1A**), which indicates that high expression of Cx43 is associated with scar formation. Quantification of relative Cx43 intensity showed that relative Cx43 intensity was significantly increased in keloid compared to normal skin (**Fig. 4.1B**). Trichrome staining showed compact and fibrotic collagen patterns compared with normal skin (**Fig. 4.1C**). Therefore, the expression pattern of Cx43 implied that Cx43 played a pivotal role in scar formation.
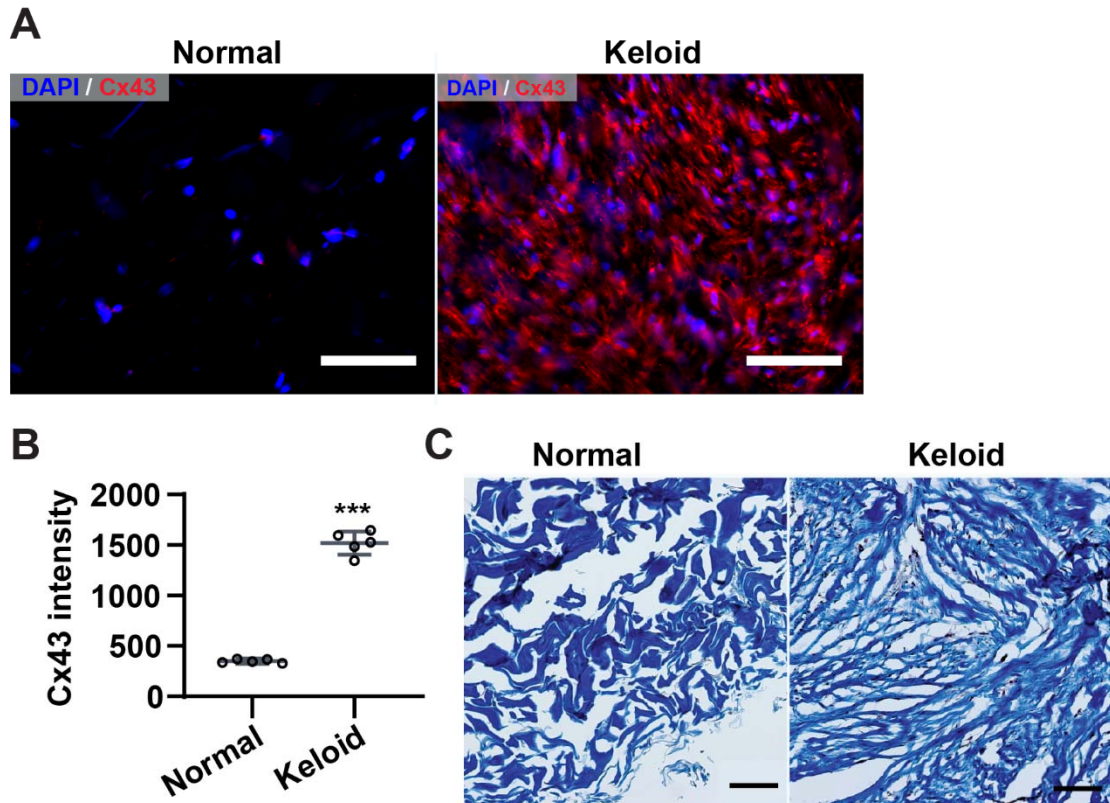
Figure 7.1   Cx43 on human normal skin and keloid. (**A**) Immunofluorescence staining of Cx43 (red) in human normal skin and keloid. DAPI (blue) was counterstained to profile nuclei. (**B**) Quantification of fluorescence intensity of Cx43 in figure (**A**. **C**). Masson's trichrome staining of the cryosections from human normal skin and keloid. Mean ± SEM, n = 5, unpaired two-tailed student's *t*-test, ***, p < 0.001. Scale bars = 100 μm.

7.1.2 Compact collagen deposition in skin-fascia explants

A whole skin-fascia explant undergoes skin contraction with scar formation outside the animal is one novel model which describes scarring very well *in ex vivo*. Briefly, skin-fascia explants were created from the back-skin from En1^{Cre};R26^{mTmG} mice, double transgenic reporter mice in which scar-prone fibroblast, EPFs in contrast with remaining fibroblasts, ENFs, contributing to scar formation, which allowed us to track both two functionally distinct fibroblastic lineages in genuine whole skin conditions in high detail and throughout the wound repair process. Skin-fascia explants cultured

for 5 days developed typical scars with denser plug of collagen fibres, as compared to fresh day 0 skin-fascia explants (**Fig. 4.2A,A', 4.2B**). Based on quantification of area of collagen fibres, cultured explants in day 5 was around 4 times higher than fresh tissue (**Fig. 4.2B**).
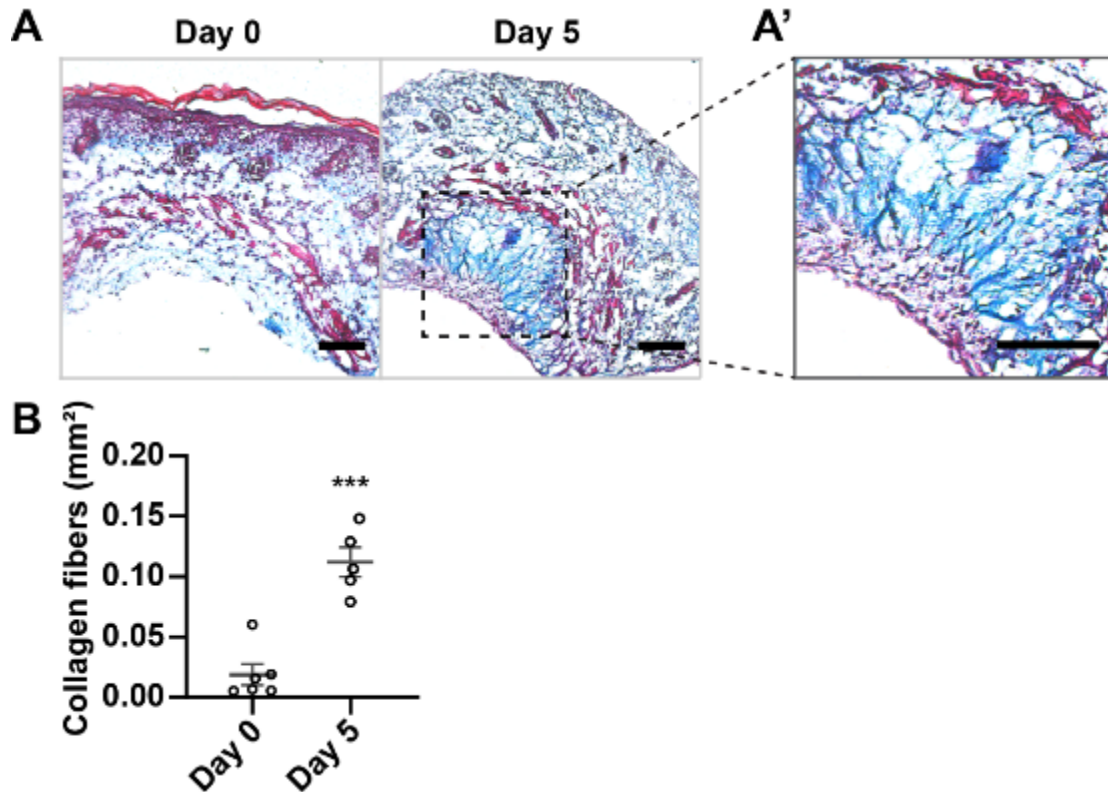
Figure 7.2   Collagen deposition in murine skin-fascia explants. (**A**) Masson's Trichrome staining of cryosections of a Day 0 and a Day 5 skin-fascia explants. (**A'**) Magnification of scar area in Day 5 skin-fascia explants. (**B**) Quantitative collagen fibres in scar areas of Day 0 and Day 5 skin-fascia explants. Mean ± SEM, n = 5, unpaired two-tailed student's *t*-test, ***p < 0.001. Scale bars = 100 μm.

7.1.3 Cx43 expression in skin-fascia explants

Regarding our well-established skin-fascia explants model, Cx43 distribution in tissue was observed subsequently. In the immunostaining section, Cx43 was specifically upregulated in EPFs along within the scar area; Cx43 was completely

absent from EPFs in healthy skin (**Fig. 4.3A, A'**). Quantification of relative Cx43 intensity showed significant increased intensity on skin-fascia explants compared to day 5 and day 0 (**Fig. 4.3B**).
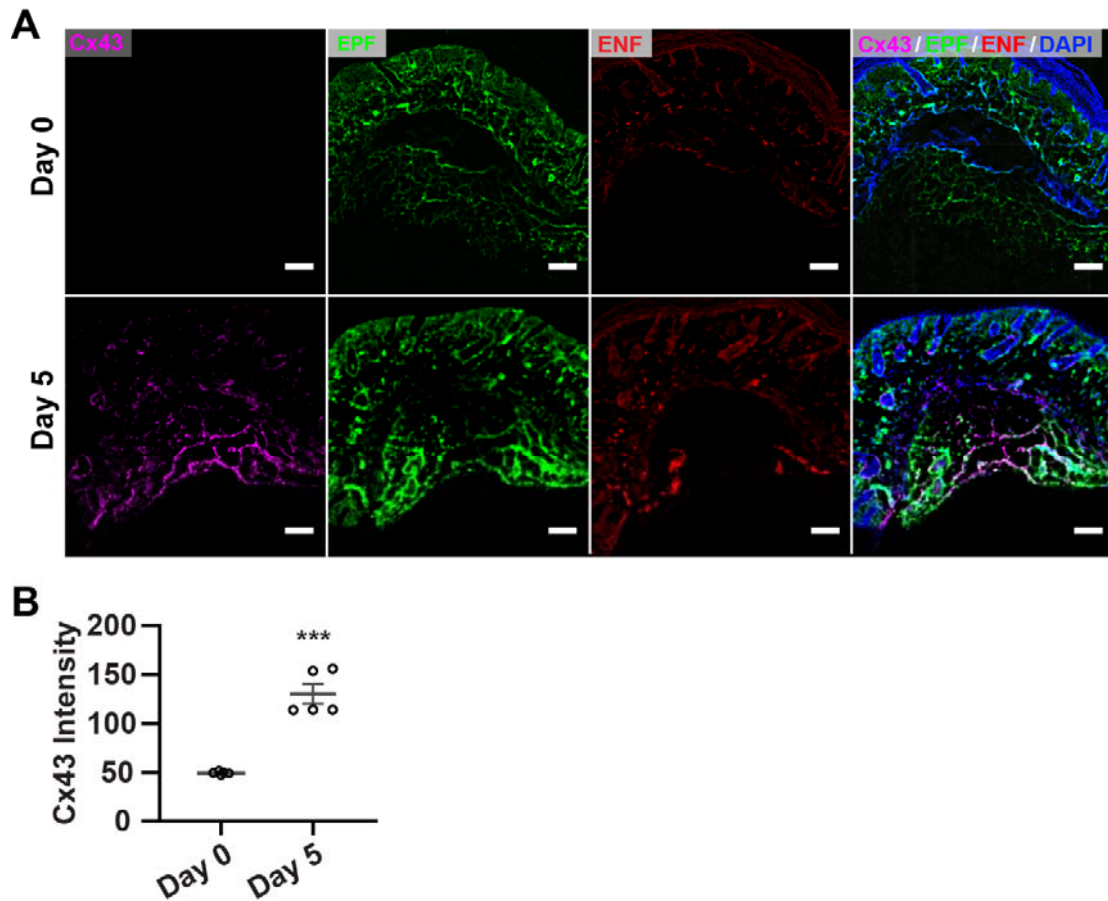
Figure 7.3   Cx43 expression in murine skin-fascia explants.

(**A**) Immunofluorescence staining of Cx43 (magenta) in a day 0 and a day 5 skin-fascia explant from the back-skin of En1^{Cre};R26^{mTmG} mice. EPFs are green, other cells are red, nuclei are blue. (**B**) Quantification of fluorescence intensity of Cx43 in explants at days 0 and 5. Mean ± SEM, n = 5, unpaired two-tailed Student's t-test, ***$p < 0.001$. Scale bars = 100 μm.

7.1.4 Multiphoton microscopic analyses of Cx43 expression on skin-fascia explants

To visualize furtherly EPF lineage-specific expression of Cx43 in more detail, we performed whole-mount 3D immunolabelling of the skin-fascia explants at Day 5. Cx43 expressed on the skin-fascia explants in 3D imaging, in which explants containing EPFs and ENFs were punched off from En1^{cre};R26^{mTmG} double transgenic mice dorsal skin (**Fig. 4.4A**). In addition, whole skin was undergoing contraction with scar formation, which revealed EPFs collectively expressed Cx43, as a whole population. Taken last Cx43 immunostaining together, Cx43 mainly distributed on the centre area of skin-fascia explants tended to co-localizing with EPFs which are primary fibroblast lineage contributing to scar formation (Rinkevich et al., 2015).
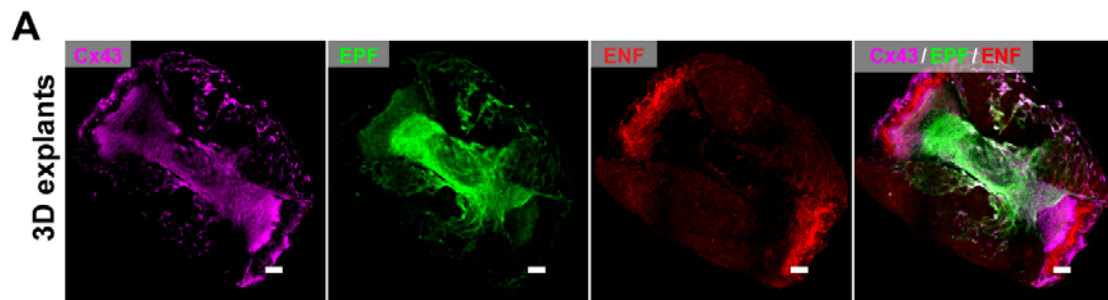
Figure 7.4   Multiphoton microscopy analyses Cx43 expression on skin-fascia explants. (**A**) 3D immunolabelling of Cx43 in skin-fascia explants from the back-skin of En1^{cre};R26^{mTmG} mice were imaged by multiphoton microscopy, in which Cx43 was stained as magenta, EPFs indicated as green, ENFs as red. Scale bars = 100 μm.

7.1.5 Cx43 expression in *in vivo* wounds

To analyse the physiologic relevance of expression patterns of Cx43 during wound healing in *vivo* with our findings, full-thickness excisional wounds on the back skin of En1^{cre};R26^{mTmG} double transgenic mice were operated and the protein expression of

Cx43 on histologic slides of these wounds were analysed. Cx43 protein expression in live mice completely mirrored and overlapped with the patterns of expression we initially found using ex vivo skin-fascia explants. Wounds samples from adult mouse dorsal skin were collected post wounding at day 0, 3, 5 and 7. Protein expression was absent from healthy skin, and was unregulated upon wounding in both epidermis and wound bed. In wound bed, Cx43 was exclusively expressed in fascia EPFs, peaking at 5 days post-wounding, and co-localizing with fascia EPFs during the later steps of the wound healing process (**Fig. 4.5A, B**). Collectively, these results demonstrate that Cx43 is exclusively expressed in scar-progenitor EPFs, during wound healing and may function in these cells to control connective tissue matrix outpouring and scar severity.
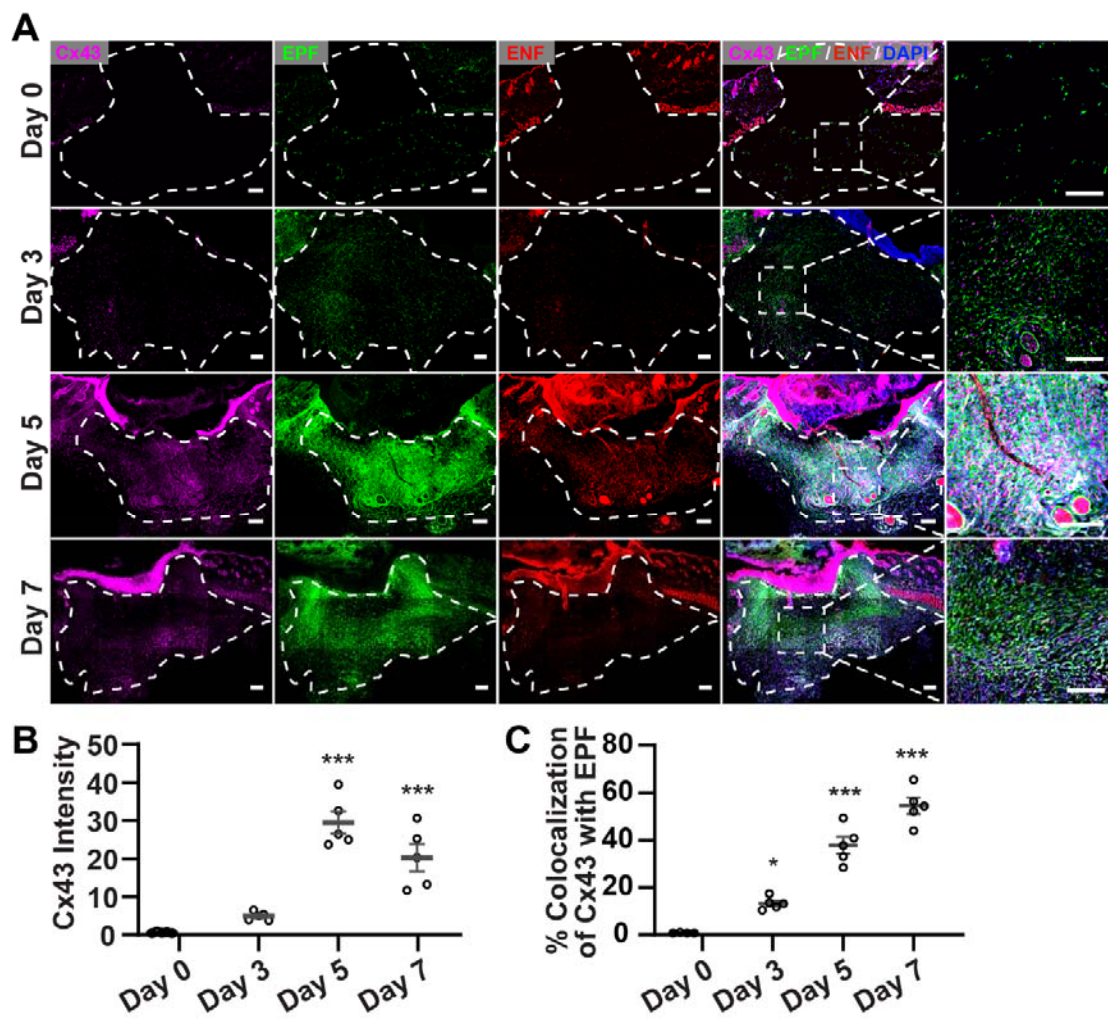
Figure 7.5   **Cx43 expression on wounds *in vivo*.** Wounds on En1cre;R26mTmG adult mouse dorsal skin were collected post wounding at days 0, 3, 5, and 7. (**A**)

Immunostaining of cryosections showed Cx43 expression zone (magenta) at dorsal skin. EPFs were shown in green. Nuclei were stained with DAPI (blue). Dashed lines indicate the border of the wound bed. Right column shows high magnification of white dotted line in wound area. (**B, C**) Quantification of fluorescence intensity of Cx43 (B) and percentage of co-localization of Cx43 with EPF (**C**) in wounds on days 0, 3, 5, and 7 post-wounding. Mean ± SEM, n = 5, one-way ANOVA with Tukey's multiple comparison. ***, $p < 0.001$. Scale bars = 200 µm.

7.2   Inhibition of Cx43 reduces scar formation.

7.2.1 Gap junction inhibitors reduce scar formation on skin-fascia explants

We next investigated the function of Cx43 on wound healing and scar formation with skin-fascia explants *ex vivo*. We harvested whole skin explants and treated with 2-APB, a small molecule that shuts down gap junction-mediated cell communications by increasing Cx43 degradation(Yang et al., 2011) and the small molecule GAP 27, a reversible peptide-mimetic blocker that selectively targets the second extracellular loop of Cx43 (Evans and Leybaert, 2007). To place the gap junction phenotypes in relation to known scar modulators, we also included TGF-β1 treatment in our agent panel, as a characterized fibrosis inducer (Yun et al., 2019) and the TGF-β1 inhibitor SB431542 (Inman et al., 2002; Jiang et al., 2020), which was used as a control for reducing scar severity. As expected, skin-fascia explants treated with 10 ng/mL TGF-β1 had severe and larger scars with more abundant collagen plugs at wound centres than control explants cultured in media alone. More importantly, 1 µg/mL 2-APB or 8 µM GAP 27 significantly reduced scar area, collagen deposition content, and expression of EPF marker CD26, which was comparable to those found in skin explants that were exposed to TGF-β1 inhibitors (**Fig. 4.6A, B**).

A

	BF	Trichrome	CD26 / DAPI
Ctrl			
TGF-β1			
SB431542			
2-APB			
GAP 27			

B

Scar area (mm²)

Ctrl, TGF-β1, SB431542, 2-APB, GAP 27

C

CD26 intensity

Ctrl, TGF-β1, SB431542, 2-APB, GAP 27
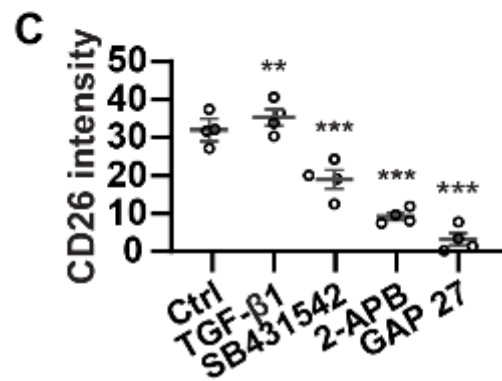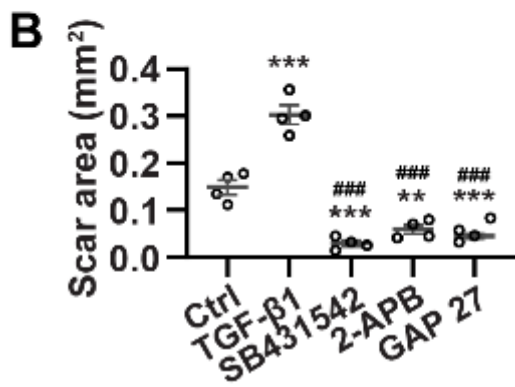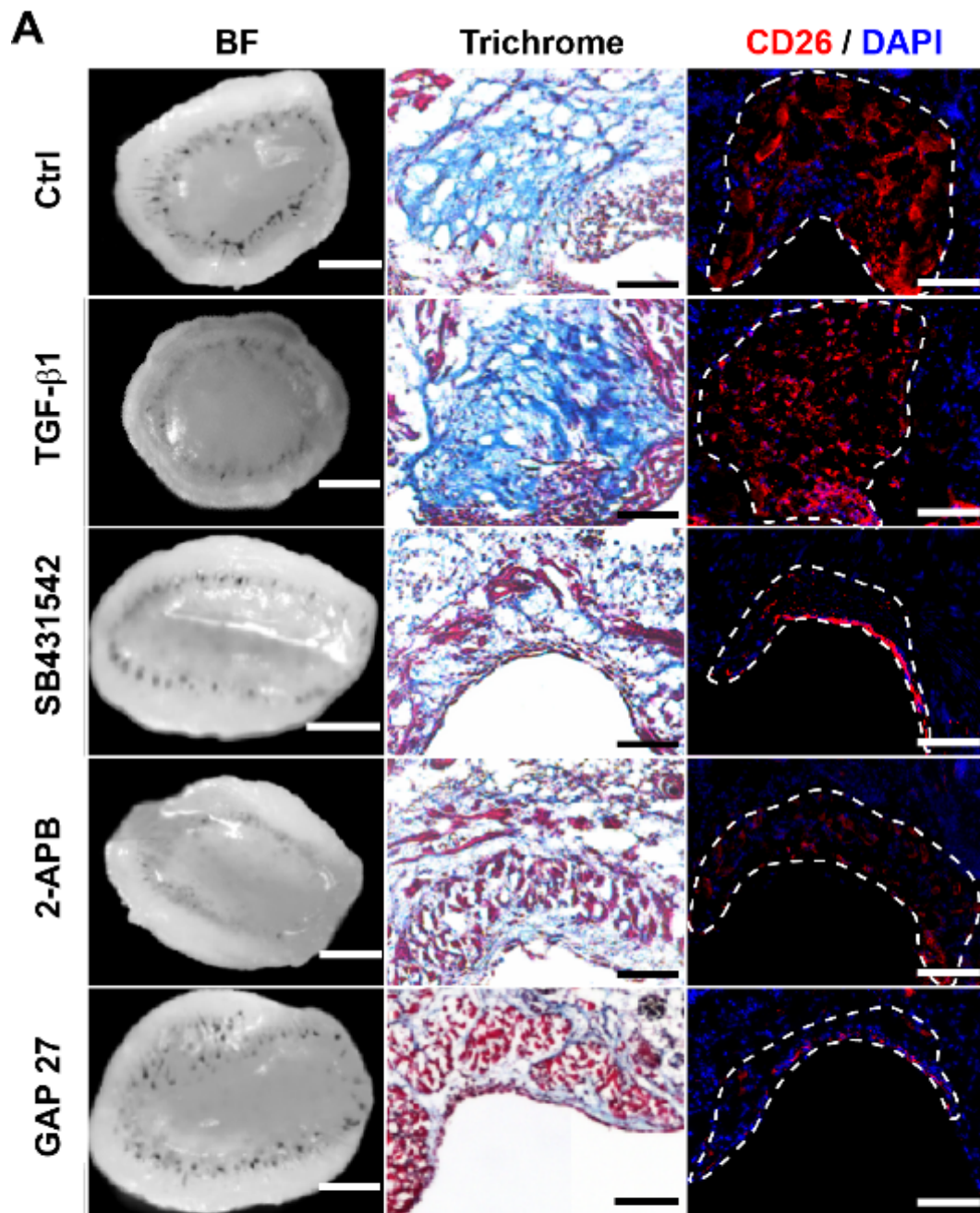
Figure 7.6   Inhibiting gap junction reduced scar formation on skin-fascia explants. (**A**) Skin-fascia explants were cultured for 5 days with 10 ng/mL TGF-β1 as positive control, 2 µM SB 431542, 1µg/mL 2-APB, or 8 µM GAP 27, respectively. Whole-mount bright-field images of skin-fascia explants (left panel), Masson's Trichrome staining of cryosections (middle panel) and immunostaining of CD26 (red) (right panel) were shown. Dashed lines indicate the scar areas corresponding to Masson's trichrome staining. (**B**) Quantitative analysis of scar areas in Masson's trichrome stained sections. (**C**) Quantification of fluorescence intensities of CD26 in scar. Mean ± SEM, n = 4. One-way ANOVA with Tukey multiple comparisons. Scale bars: left panel of (**A**) = 500 µm, middle and right panel (**A**) = 100 µm.

7.2.2 Gap junction inhibitors reduce Cx43 expression on EPFs

To verify the relation of Cx43 expression on EPFs and collagen deposition, EPFs were FACS-sorted from back-skin of adult En1[cre];R26[mTmG] mice by negative selection with lineage markers (CD31, CD45, Ter119, Tie2, CD326, Lyve-1) (**Fig. 4.7A**). EPFs were treated with 10 ng/mL TGF-β1, 1 µg/mL 2-APB and 8 µM GAP 27 for 24h, following by immunofluorescent staining with collagen I and Cx43. Both 2-APB and GAP 27 significantly reduced Cx43 expression on EPFs, without significantly alteration of collagen I deposition relative to untreated cells (**Fig. 4.7B-D**).
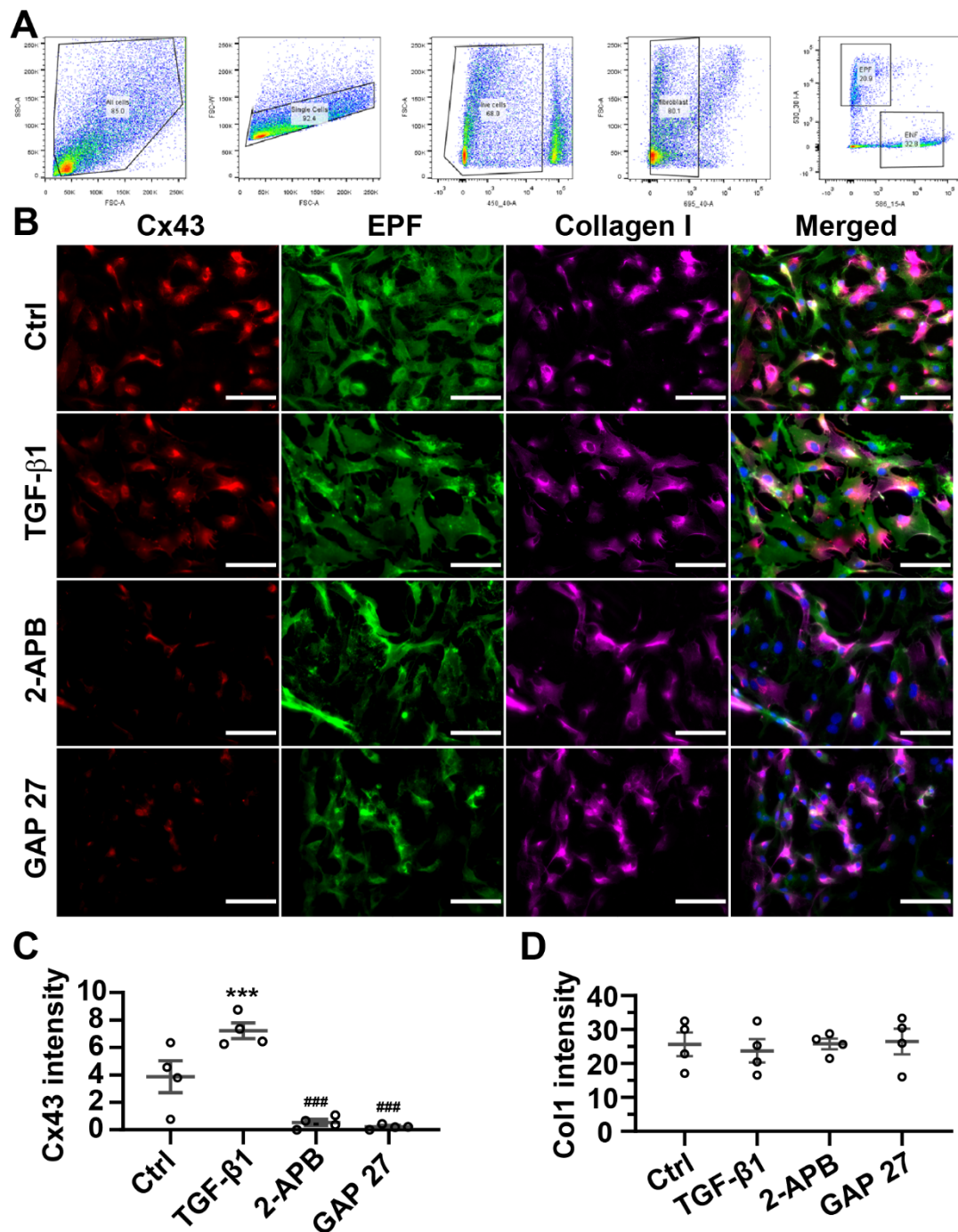
Figure 7.7 **Gap junction inhibitors reduce Cx43 expression on EPFs but no**

collagen I. (**A**) FACS gating strategy for EPFs by negative selection with lineage

markers (CD31, CD45, Ter119, Tie2, CD326, Lyve-1) from the back-skin of adult

En1^{cre};R26^{mTmG} mice. (**B**) FACS-sorted EPFs were cultured with 10 ng/mL TGF-β1, 1

μg/mL 2-APB, or 8 μM GAP 27 for 24h, respectively. Depicted are representative

immunofluorescence images Cx43 (red) and Collagen I (magenta) on EPFs (green).

Nuclei are stained with DAPI (blue). (**C**, **D**) Quantification of fluorescence intensities of Cx43 (**C**) and Collagen I (**D**) showed in (**B**). Mean ± SEM, n = 4, one-way ANOVA with Tukey's multiple comparison. *, $p < 0.05$; **, $p < 0.01$; ***, $p < 0.001$. Scale bars = 100 µm.

7.2.3 Gap junction inhibitors reduce scar formation in splinted full-thickness wounds *in vivo*

To further address the role of gap junction in EPFs during physiologic wounds *in vivo*, we generated full-thickness excisional wounds on the back of adult mice. The wounds were splinted with silicone rings to minimize the muscle contraction. We then employed a splinted wound model by suturing silicone rings to the periphery of the wound, thereby mimicking human deep wounds by minimizing muscle contraction. We then injected 60 µL of 0.1% DMSO as control, or 60 µL of 2-APB (at 4 µg/ mL) or 80 µM GAP 27 was subcutaneously around the wound on every other day and monitored wound closure and scar formation *in vivo*. With both drugs tested, scar tissues that were harvested on day 21 post-wounding were significantly smaller, in both area and depth compared with the DMSO control group (**Fig. 4.8A-C**). Less CD26 expression and collagen content were observed in the inhibitory groups (**Fig. 4.8A, 4.8D, 4.8E**). These data reveal that Cx43 is essential in EPFs to orchestrate proper scar formation in wounds.
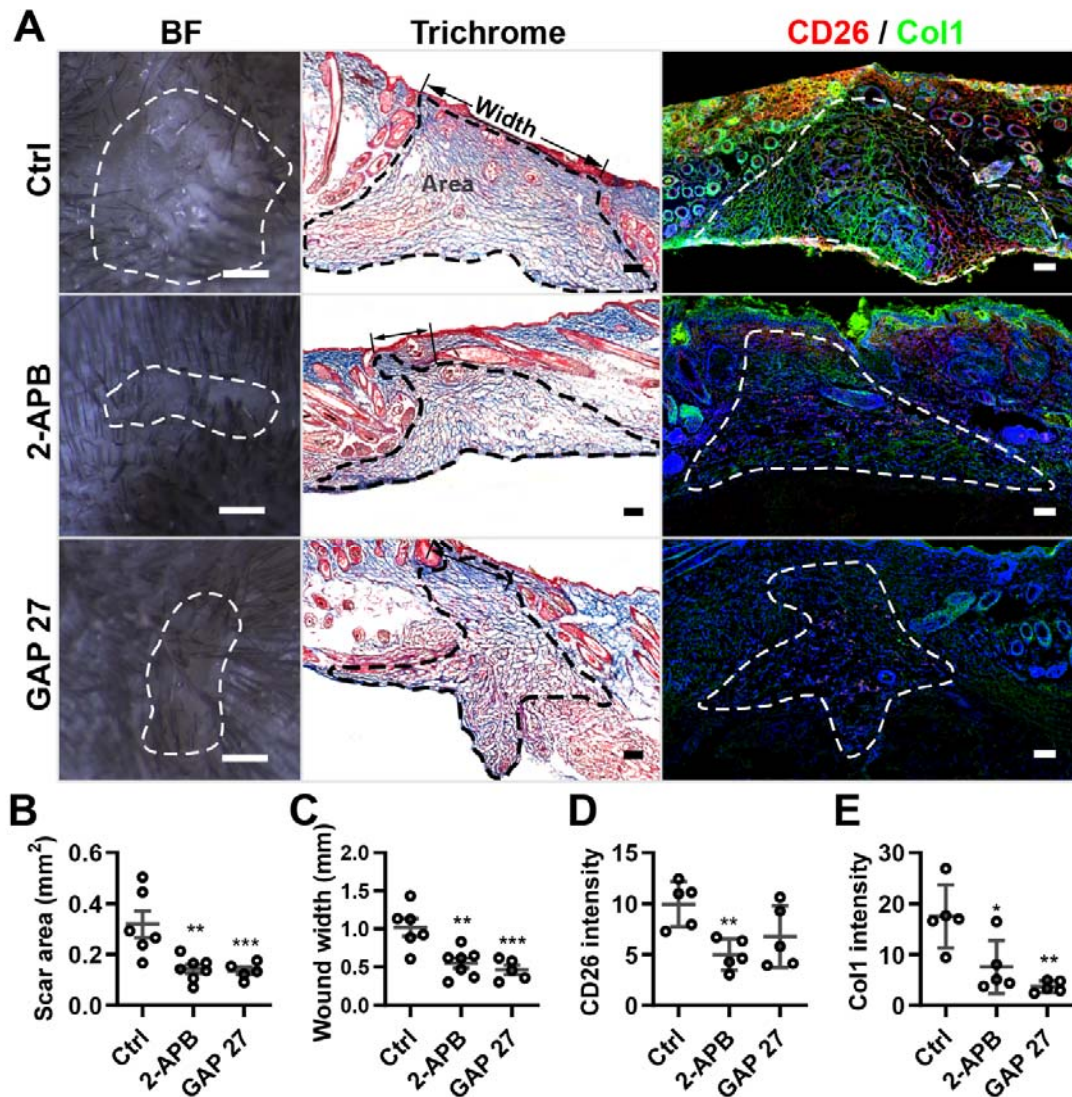
Figure 7.8 Gap junction inhibitors reduce scar formation on splinted wounds *in vivo*. (**A**) Splinted wounds were subcutaneously injected with 60 µL of 2-APB at 4 µg/mL, GAP 27 at 80 µM, or control on every second day. Scars were harvested at day 21 post-wounding. Macroscopic scar photos (BF), Masson's trichrome stained wound sections, and immunostaining of CD26 (red) and Collagen I (green) are shown, nuclei are stained with DAPI. Dash lines outline the scar area, and arrows indicate the scar width. (**B**, **C**) Quantitative analysis of scar area and scar width. (**D**, **E**) Quantitative analysis of fluorescence intensities of CD26 and Collagen I. Mean ± SEM, n = 5, one-way ANOVA with Tukey's multiple comparison. *p < 0.05, **p < 0.01, ***p < 0.001. Scale bars: A (left panel) = 500 µm; A (middle and right panel) = 100 µm.

7.3 Disrupted calcium oscillation by gap junction inhibition underlies the reduced scarring

7.3.1 Gap junction inhibitors disturb the functional communication on fibroblasts.

Gap junctions, hexametric connexin hemi-channels sensitive to intracellular calcium, pH, cholesterol and phosphorylation events, allow for the passage of cytoplasmic small molecules between cells (Chen et al., 2016; Wong et al., 2016). To understand in more detail how Cx43 regulates EPF behaviour in wounds, we first looked into the function of gap junctions in cell-cell communication by looking into the intercellular passage of small molecules. Fibroblasts were treated with calcein-AM ester, a membrane permeable dye that can be hydrolysed to calcein by cellular esterase (Kiang et al., 1994). Following cleavage, the fluorescent calcein is retained inside the cell and can be transferred to other cells through gap junction channels alone, thereby providing a fluorescence marker system to check for intercellular communications. We mixed calcein labelled fibroblasts with unlabelled fibroblasts at a ratio of 1: 10 and documented the transfer of calcein from labelled cells to unlabelled cells by time-lapse imaging (**Video 1**). We found that adding Cx43 inhibitor 2-APB in culture media substantially suppressed calcein transfer (**Fig. 4.9A**), as indicated by significant slower increase of calcein fluorescence in unlabelled fibroblasts with 2-APB treatment compared to control condition (**Fig. 4.9A, B**). Moreover, the treatment with GAP 27 completely abolished calcein transfer to the unlabelled fibroblasts (**Fig. 4.9A, B**). Relative intensity (F_x / F_0) of transfected cells under 2-APB was linear growth and with GAP 27 was almost horizontal coming to the plateau on 30 min compared to exponential growth in the control group (**Fig. 4.9B**).
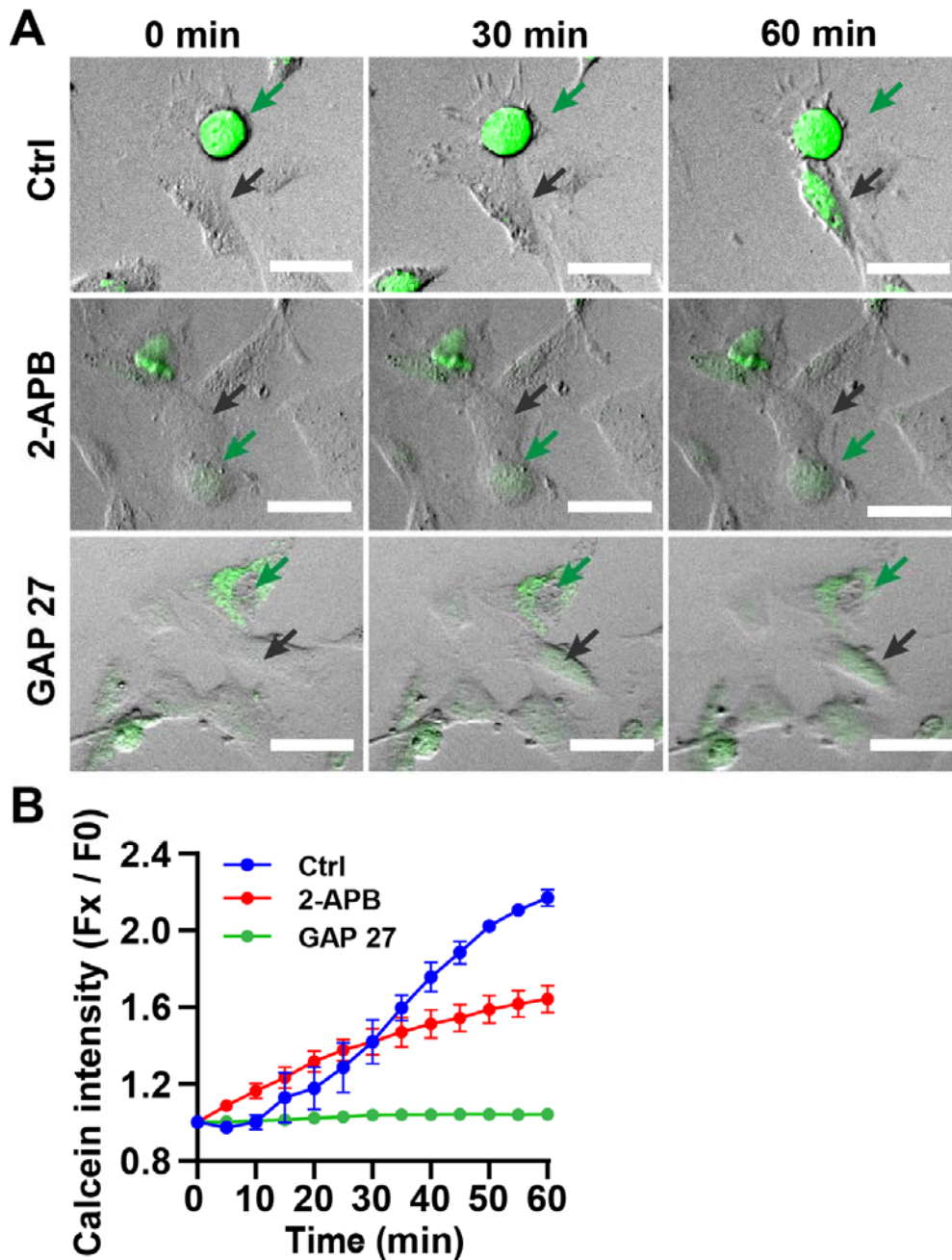
Figure 7.9   Gap junction inhibitors disturb the calcein AM transportation. (**A**) Snapshots of time-lapse imaging of calcein dye (green) transfer between calcein AM labelled 3T3 fibroblasts and unlabelled fibroblasts at 0 min, 30 min and 60 min. 3T3 fibroblasts were cultured in control medium or medium containing 1 μg/mL 2-APB or 8 μM GAP 27. Green arrows indicate the calcein AM labelled 3T3 fibroblasts, and black arrows indicate the originally unlabelled recipient fibroblasts. (**B**) Ratio of calcein intensity in unlabelled fibroblasts at the indicated time point (F_x) to the beginning of

recording (F_0) in the control condition, or in the presence of 2-APB or GAP 27. Mean ± SEM, n = 3, unpaired two-tailed Student's *t*-test, ***p < 0.001. Scale bars = 50 μm.

7.3.2 Gap junction inhibitors interrupt calcium oscillation on fibroblasts.
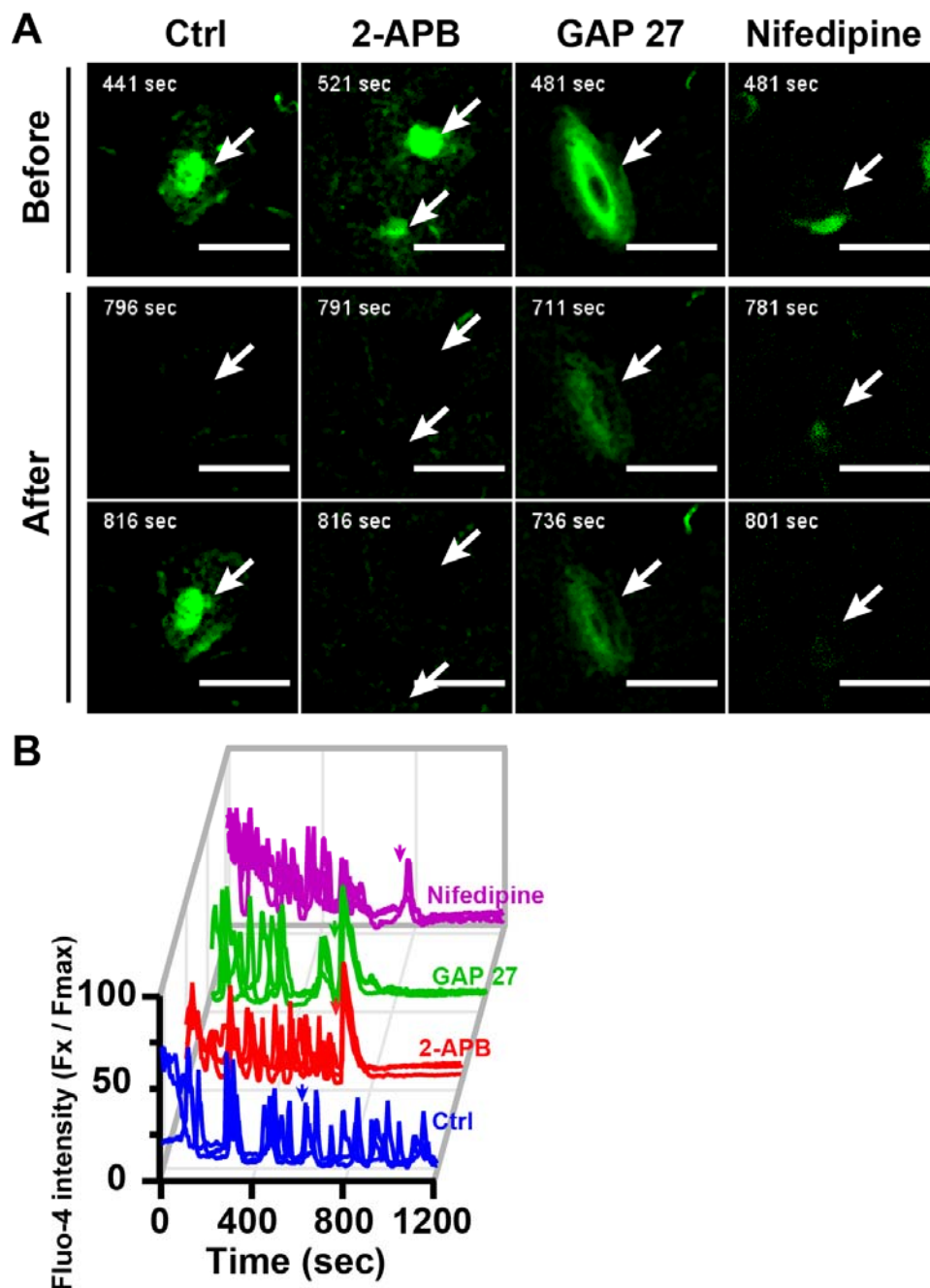
Figure 7.10   Gap junction inhibitors interrupt calcium oscillation on fibroblasts.

(**A**) Snapshots of time-lapse imaging of Fluo-4 AM labelled 3T3 fibroblasts at indicated

time before and after the treatment of 1 µg/mL 2-APB, or 8 µM GAP 27, or 1 µM Nifedipine. White arrows indicate the obvious active cells. Fluo-4 AM dye was shown in green. (**B**) Ratio of fluorescence intensities of Fluo-4 in fibroblasts at the indicated time points (F_x) to the maximum recording (F_{max}) were plotted over time (0 ~ 1200 s) before and after the treatment with 2-APB, GAP 27, or Nifedipine. Mean ± SEM, n = 5, unpaired two-tailed Student's *t*-test, ***p < 0.001. Scale bars = 50 µm.

Calcium waves transduce signals that propagate and spread to nearby fibroblasts and are tightly controlled by gap junctions (Cotrina, 1998). Given that calcium plays a pivotal role for the tissue homeostasis and wound healing (Lembong et al., 2017), to address whether gap junction inhibition on scar formation involved calcium signalling, we went on to investigate the role of Cx43 in regulating calcium signalling during scar formation. By using a calcium indicator Fluo-4 AM dye coupled with time-lapse imaging, long-lasting periodic calcium oscillations were observed in cultured fibroblasts (**Video 2**). This calcium wave was inhibited by a broad-spectrum calcium channel blocker Nifedipine at 1 µM (**Fig. 4.10A, B**). Intriguingly, Cx43 inhibitors, 2-APB at 1 µg/mL and GAP 27 at 8 µM, blocked calcium oscillation, identical to Nifedipine treatment (**Fig. 4.10A, B**). These data indicate that intercellular passage of Ca^{2+} among fibroblasts and the subsequent calcium signal oscillation is controlled by Cx43 gap junctions. Our results are consistent with gap junction blocking, such as octanol and DSA dramatically disrupting calcium wave propagation (Benninger et al., 2008; toshihiko, 1998).

7.3.3 Calcium inhibitor reduces scar formation on skin-fascia fascia.

To link calcium signalling, with gap junction and scar formation, the effect of Nifedipine on scarring was assessed within skin-fascia explants ex vivo and wounding *in vivo*. Similar to 2-APB and GAP 27, explants treated with 1 μM Nifedipine showed significantly less collagen deposition (**Fig. 4.11A**) and smaller scar area (**Fig. 4.11B**). The results hinted that blocking calcium signalling could be a mechanism under the healing role of gap junction.
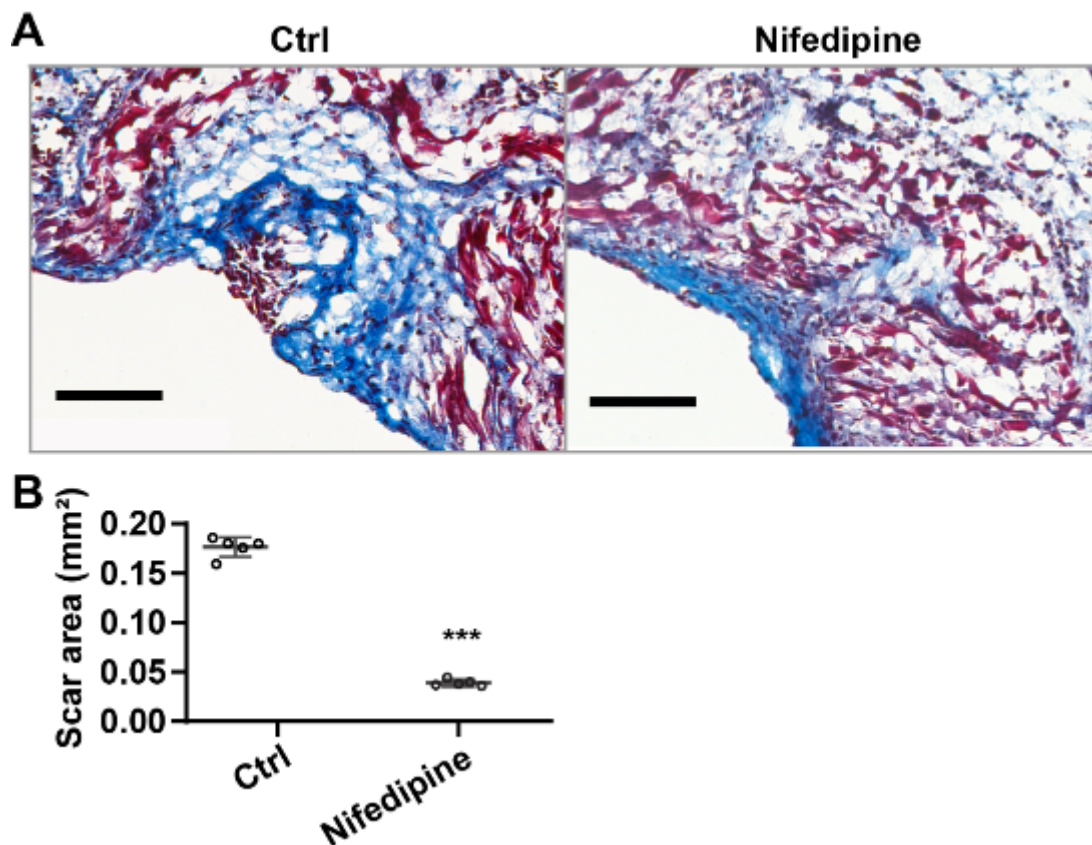
Figure 7.11   Calcium blocker reduces scar formation on skin-fascia fascia. (**A**) Representative images of Masson's trichrome staining of control or 1μM Nifedipine treated skin-fascia explants. (**B**) Quantitative analysis of scar area in A. Mean ± SEM, n = 5, unpaired two-tailed Student's *t*-test, ***, P< 0.001. Scale bars = 100 μm.

7.3.4 Calcium inhibitor reduces scar formation *in vivo*

To further resolve the role of calcium signalling in scar formation *in vivo*, excisional wounds and splinted rings were operated on mice followed by a 21-days course of Nifedipine treatment. Moreover, subcutaneous injection of 60 µL Nifedipine at 10 µM resulted in less collagen deposition, apparent smaller scars area *in vivo* compared to vehicle group (**Fig. 4.12A-C**). Collectively, these results revealed that these results indicate that Cx43 gap junctions are needed to maintain calcium signal oscillations in EPFs that underlie the scarring response.
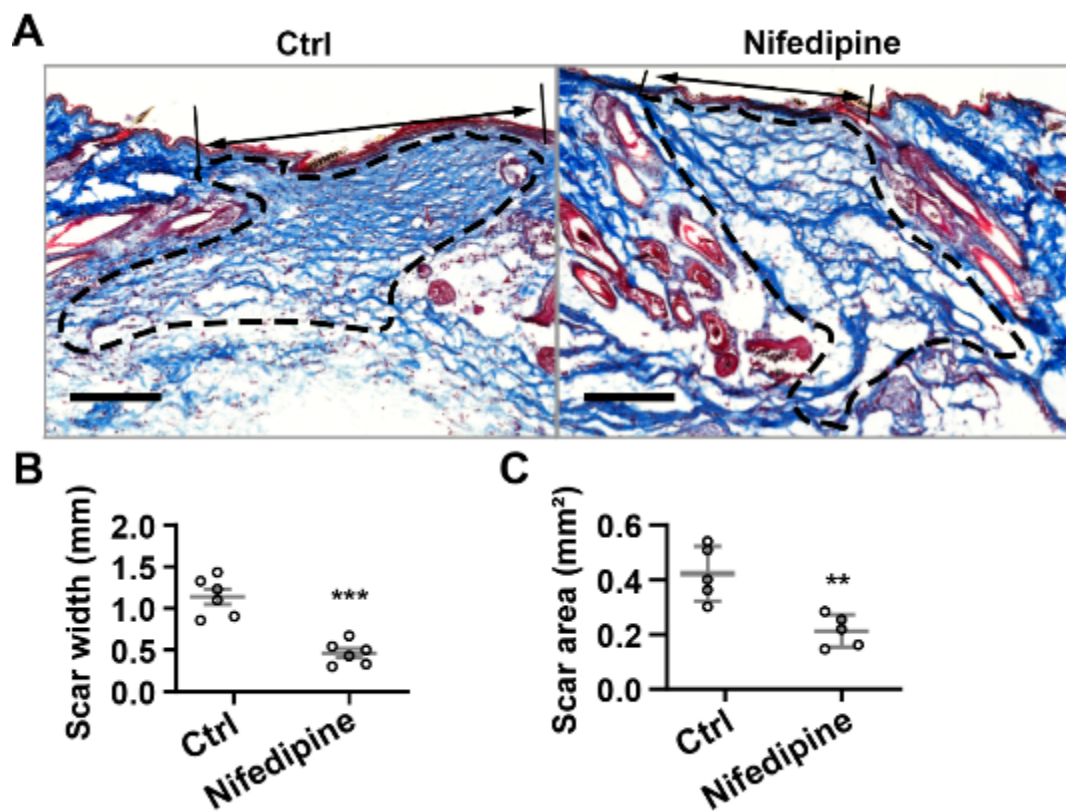
Figure 7.12   Calcium inhibitor reduces scar formation *in vivo*. (A) Masson's trichrome stained sections from adult mice splinted wounds at day 21 under Nifedipine treatment compared to DMSO control treatment. (**B**, **C**) Quantitative analysis of car width (**B**) and scar area (**C**) of figure A. Mean ± SEM, n = 5, unpaired two-tailed Student's *t*-test, *, $P<0.05$; **, $P< 0.01$; ***, $P< 0.001$. Scale bars = 200 µm.

7.4 Inhibition of Cx43 abrogates EPF swarming and fascial matrix migration

7.4.1 EPF swarming were abrogated by Cx43 inhibition on skin-fascia explants

To investigate in more depth, the possible effect of Cx43 inhibition on EPFs behaviour during wound healing, we analysed the complete migration dynamics of EPFs in the presence of the Cx43 gap junction blocker GAP 27 or calcium channel blocker Nifedipine. We crossed En1^{Cre} and H2B-mCherry reporter mice and isolated whole skin explants from the back-skin of En1^{Cre};R26$^{LSL-H2B-mCherry}$ double transgenic mice. In these mice, EPFs express nuclear mCherry and allow computational tracking of individual fibroblasts. **Videos 3-5** shows the migration tracks of EPFs in control, GAP 27, and Nifedipine treated explants, respectively. In control explants, EPFs collectively migrated towards wound centres (**Fig. 4.13A, Video 3**). By contrast, GAP 27 or Nifedipine treatment caused distinct EPF clusters to disaggregate from wound centres into the edges of the wound tissue, indicative of a lack of collective behaviour (**Fig. 4.13A, Video 4, 5**). Furthermore, computational analysis of EPF tracks showed that, while EPF migration was directional towards wound centres in control explants, both gap junction inhibition and calcium inhibition caused EPFs dispersing randomly and migrating at significantly reduced speeds (**Fig. 4.13B, C**).
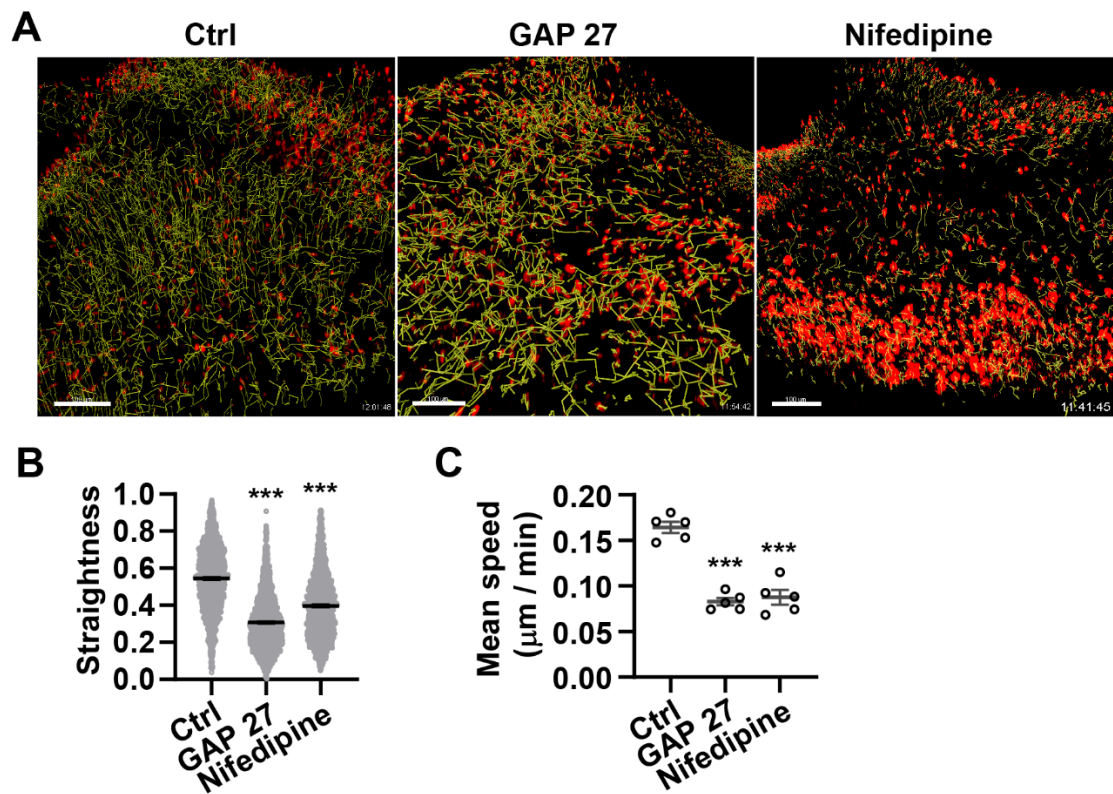
Figure 7.13   EPF swarming was abrogated by Cx43 inhibition on skin-fascia explants. (**A**) Tracking of EPFs from live imaging of control or 8 μM GAP 27 treated or 1 μM Nifedipine treated skin-fascia explants, made from back-skin of En1[Cre]; R26 [LSL-H2B-mCherry] nuclear reporter mice. (**B**) Straightness analysis of EPF tracks in control, GAP 27 treated or Nifedipine treated skin-fascia explants. Value 0 presents irregular movement, and 1 indicates definitive straightness migration, horizontal line represents the mean of all cells. (**C**) Mean speed of EPF migration in control SCADs versus GAP 27 treated, Nifedipine treated SCADs. Mean ± SEM, n = 5, one-way ANOVA with Tukey's multiple comparison. ***$p < 0.001$. Scale bars = 100 μm.

7.4.2 Absent collective migration by gap junction inhibition *in vivo* chimeric transplantation model

Scar tissue is mainly contributed by subcutaneous fascia, in which the movement of fascial matrix and EPFs is a key step for scarring (Correa-Gallegos et al., 2019). To further address how Cx43 inhibitors interfere with fascia and EPFs movement into

wounds, chimeric skin to trace the fascia was created by combining the fascial layer from R26$^{VT2/GK3}$ back skin with epidermal and dermal layer from R26^{mTmG} back skin. In this chimeric skin, fascia cells all express GFP whereas dermal cells all express RFP. A 2 mm full-thickness excisional wound was created in the centre of the chimeric skin graft, and transplanted to fresh excisional wounds on the back of Rag$^{2-/-}$ immunodeficient mice in order to circumvent graft allogeneic rejection. Thereafter, 60 µL of GAP 27 at 80 µM or 60 µL of control PBS was subcutaneously injected around the chimeric graft, and scar tissue was harvested 14 days later (**Fig. 4.14 A**). In the control mice green cells from fascia collectively extended upwards and plugged the wounded area, whereas GAP 27-treated graft fascial cells remained in place (**Fig.4.14 B**). Quantifications of the chimera experiments showed that fascia derived matrix covered 73% of control wounds, but only 11% in GAP 27 treated wounds (**Fig. 4.14 C**).
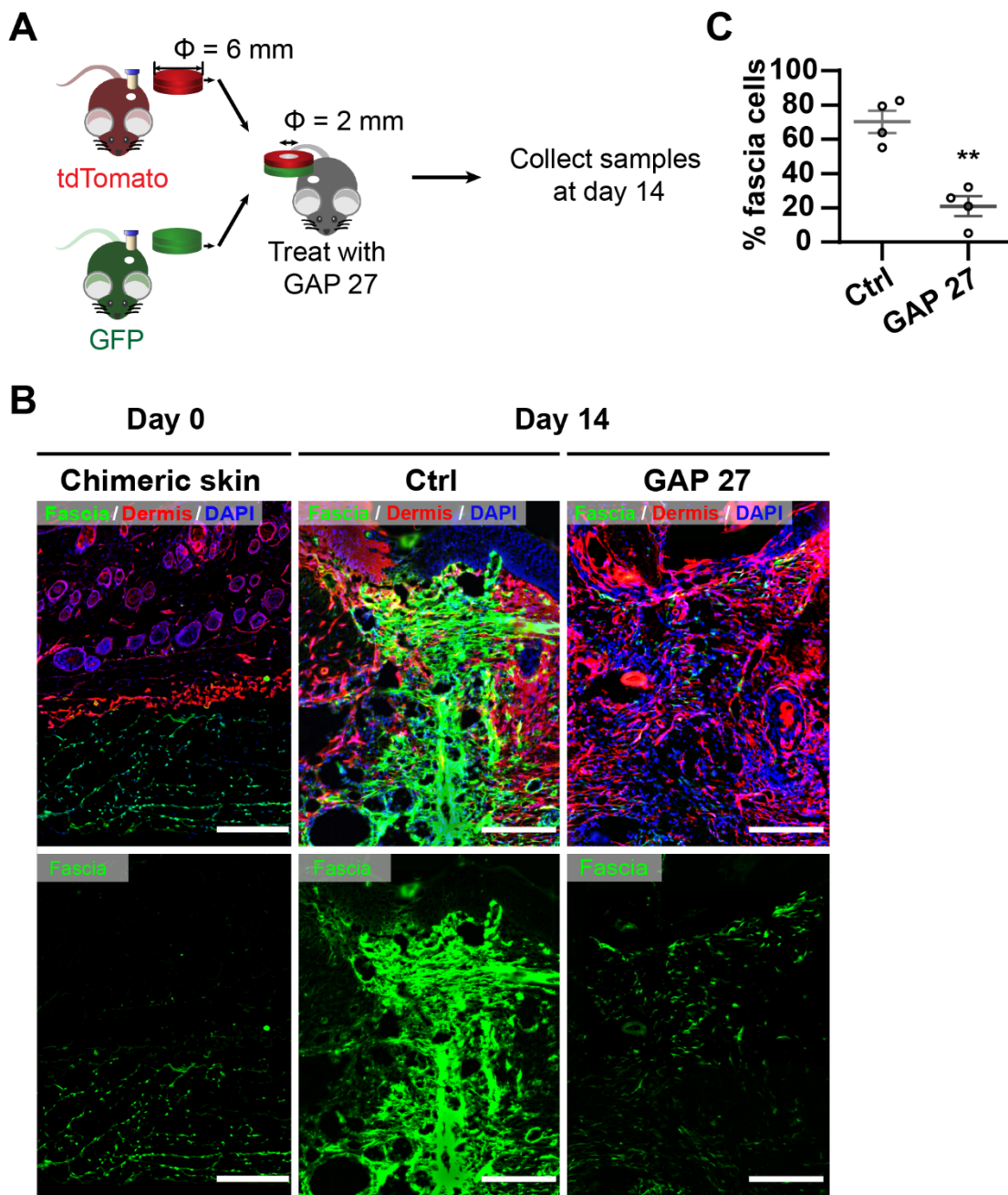
Figure 7.14   Absent collective migration in chimeric transplantation model by gap junction inhibition *in vivo*. (**A**) Scheme of chimeric skin graft transplantation. (**B**) Fluorescence images of chimeric skin graft at day 0 and at day 14 post-wounding under control PBS or GAP 27 treatment. Fascia cells are in green and dermal cells are in red. (**C**) Percentage of fascia cells in the scar of chimeric skin graft. Mean ± SEM, n = 4, unpaired two-tailed Student's *t*-test, **$p<0.01$. Scale bars = 200 μm.

7.4.3 Matrix movement was inhibited in labelled matrix tracing in situ

We then set out to find if the collective migration of EPFs drives fascia matrix outpouring that plug open wounds with scars. We labelled the fascia matrix by directly injecting NHS-fluorescein into the subcutaneous space of the back skin, followed by creating full-thickness excisional wounds. GAP 27 or control PBS was subcutaneously injected around wounds. Wounds were harvested and analysed at day 7 post-wounding (**Fig. 4.15A**). In control wounds, 73.3 % wound matrix was derived from fascia. Whereas in the GAP 27 treated wounds, labelled fascia contributed only 37.9 % of the matrix normally found in wounds (**Fig. 4.15B, C**), reduced numbers of fascial EPFs as determined by CD26$^+$ and α-SMA$^+$ immunolabeling (**Fig. 4.15B, 4.15D, 4.15E**), and reduced numbers of F4/80$^+$ macrophages, as compared to control wounds.

Collectively, our experiments show that Cx43 gap junction is exclusively upregulated in fascia EPFs and that gap-junction mediates their collective migrations needed for matrix outpouring from the fascia upwards into wounds to form scars.
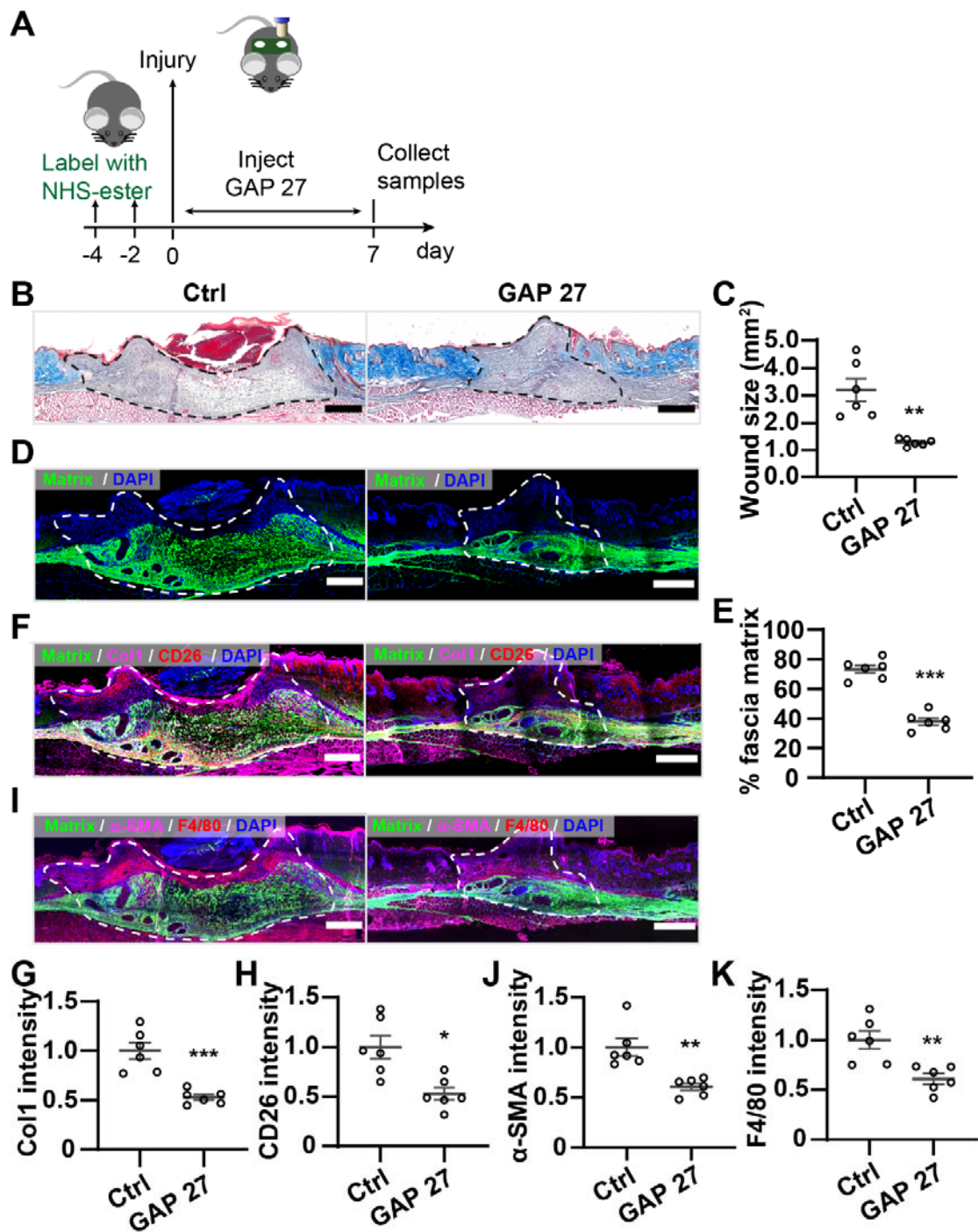
Figure 7.15   Matrix movement was inhibited in labelled matrix tracing in situ.
(**A**) Scheme of splinted wound model with prelabeled fascia matrix with NHS-fluorescein. Wounds with NHS-fluorescein prelabeled fascia matrix were harvested at day 7 post-wounding. (**B**) Masson's trichrome stained wound sections. (**C**) Quantitative analysis of wound size based on histology. (**D**) Fluorescence microscopic

images showing NHS-fluorescein pre-labeled matrix in day 7 wounds. Labled fascia matrix in green, nuclei in blue. Dash lines outline the wound area based on histology. (**E**) Quantitation of the percentage of labeled fascia matrix in wounds. (**F**) Immunostaining of Collagen 1 (magenta) and CD26 (red). Nuclei are blue. (**G**, **H**) Quantitative analysis of fluorescence intensities of Collagen 1 (**G**) and CD26 (**H**). (**I**) Immunostaining of α-SMA (magenta) and F4/80 (red). (**J**, **K**) Quantitative analysis of fluorescence intensities of α-SMA (**J**) and F4/80 (**K**). Fluorescence intensities were normalized to the mean fluorescence intensity of controls. Mean ± SEM, n = 6, unpaired two-tail Student's *t*-test, *p<0.05, **p<0.01, ***p<0.001. Scale bars: 500 µm.

8 Discussion

8.1 Cx43 on EPF involved in scarring.

Connexin is transmembrane complex responsible for transfer of small molecules between the cells, allowing intercellular communication, which has been demonstrated to play a primary vital role in various physiological processes, including tissue repair and remodelling upon injury. Though inhibition of Cx43 was demonstrated to improve the healing of physiological and chronic wounds (Zhou and Jiang, 2014), the unclear is that by which gap junction connexin43 and its therapeutic inhibitors affect scar formation in wounds. In this study, we uncover this by showing that Cx43 expression is substantially elevated in human and mouse wounds or scars, in line with previous studies that Cx43 is upregulated in chronic wounds (Michon et al., 2005). Furthermore, Cx43 is mainly expressed on EPFs, the main En1-lineage fibrogenic fibroblast lineage that is responsible for cutaneous wounding and scarring *in vivo* and *in vitro*. This indicated that Cx43 presence is cooperated with fibrotic, consisting of keloid with significant Cx43 expression and cell proliferation compared with normal skin. Moreover, collagen type I protein expression overlapped with Cx43, implicating that Cx43 positive EPFs are responsible for ECM deposition during wound healing.

Given that ablation of EPFs prevents cutaneous scarring, targeting Cx43 is a novel therapy to reduce scarring and fibrotic diseases. Several Cx43 blockers have been developed and demonstrated beneficial effects against tissue fibrosis. GAP 27, a highly selective mimetic peptide targeted to the first and second extracellular loop of Cx43, led to significantly decreased scar size and reduced collagen density, which is similar with 2-

APB, a small molecule blocking Cx32 and Cx43, protects against drug-induced liver injury with reduced hepatic failure [BJPD1](Patel et al., 2012). Our results support the therapeutic potential of connexin targeted to small molecules or mimetic peptides to therapy wound healing. Further preclinical work conducted with Cx43-based peptide therapeutics, including alpha connexin carboxyl terminus, a peptide mimetic of the Cx43 carboxyl terminus, reported improvements in wound healing and scar formation and have already moved on to phase III clinical trial (Montgomery et al., 2018). Therapeutics targeting connexin activity showed promise in beneficially modulating the human body's natural healing response for improved patient outcomes across a variety of injuries (Zhang and Cui, 2017).

8.2 Gap junction inhibition decrease scar formation by N-cadherin and calcium oscillations

Previous studies suggest that Cx43 and N-cadherin have a close relationship in mediating cell adhesion, polarity and directed migration (Matsuuchi and Naus, 2013). Knockdown Cx43 results in lower levels of N-cadherin, which suggested both Cx43 and N-cadherin are associated in a protein complex (Oyamada et al., 2005) Or N-cadherin-based adherent junctions are in close proximity to Cx43 gap junctions, and both are required for functional gap junction formation between fibroblasts (Govindarajan et al., 2010). Cx43 acts as transcription factor of N-cadherin (Kotini et al., 2018). Recently, by using live imaging techniques, we have demonstrated that N-cadherin leads to EPF aggregation and subsequent directed collective migration as swarms towards wound centers. Blocking N-cadherin results in reduced scarring and improved matrix lattice arrangement in both skin-fascia explants model *in ex vivo* and other model *in vivo* (Correa-Gallegos et al.,

2019). Therefore, anti-scarring effect we observed here with the Cx43 inhibition is partially through its impact on N-cadherin expression and the subsequent loss of EPFs.

Calcium oscillations have been implicated in regulating cell migration. Our current study demonstrates that inhibition of Cx43, by 2-APB or GAP 27, abolishes the periodic Ca^{2+} oscillation in fibroblasts, which is consistent with previous studies that blocking gap junctions by octanol or DSA dramatically disrupting Ca^{2+} wave propagation (Benninger et al., 2008) (toshihiko, 1998). Calcium oscillations have been implicated in regulating cell migration. For example, collective mesenchymal cell migration during chicken feather elongation is accompanied by synchronized Ca^{2+} oscillations governed by Cx43 gap junction networks. The Cx43 expression is activated by synergistic Hedgehog and WNT/beta-catenin signalling in mesenchymal cells (Li et al., 2018). Mukherjee and colleagues have shown that disrupting calcium oscillations in fibroblasts by Nifedipine attenuates bleomycin-induced pulmonary fibrosis (Mukherjee et al., 2015). Moreover, changes in intracellular Ca^{2+} also feeds back to gap junction function, as an increase of Ca^{2+} has been shown to trigger Cx32 hemichannel opening (De Vuyst et al., 2006). Altogether, this evidence suggest that Cx43 regulates calcium oscillations and N-cadherin expressions that coordinate collective EPF migration thus contributing to scarring.

8.3 Cx43 coordinates collective migrations into open wounds.

The previous view of scar formation explains wound healing in mammals through cross talking between fibroblasts and the wound granulation tissue (Gabbiani, 1998; Hinz, 2016). Recently, we have identified the spatial origin of scar tissue that the cellular

components and provisional matrix are mainly contributed by the subcutaneous fascia beneath the panniculus carnosus muscle upon skin wounding (Correa-Gallegos et al., 2019). However, the mechanism how the fascia tissue mobilized into open wounds to plug breached skin with scar tissue is unclear.

Collective migration is occurring as a cohesive, multicellular group while the junctions , based on cadherin, integrin and so on, between cells are retained over prolonged time periods, which is mainly discrepancy with individually migrating cells (Friedl et al., 2012). Forming one functional unit, collective migration, translocating active and passive mobile and non-mobile cells, is critical to developing various tissues in embryos and to metastasis in the course of tumour progression (Friedl et al., 2004; Fujimori et al., 2019). Cx43 plays a pivotal role in regulating cell migration. Cx43-deficient proepicardial cells showed faster migration rate than those expressing normal Cx43 (Francis et al., 2011). While it was also reported that Cx43-deficient neural crest cells and Cx43 expression diminished retinal neuroepithelial cells migrated slower than normal control groups (Huang et al., 1998; Pearson et al., 2005). These differences on the effects of migration may reflect diversity of cell types involved and cells migrate independently or in a communicating group (Mori et al., 2006).

With our new in chimera assays and matrix labelling practices *in vivo*, we confirm that Cx43 is essential for cell-cell communication in fibroblast of fascia swarming towards formative scar centre. The recruitment of scar-competent fibroblasts from outside wounds has enormous clinical significance. Strategies that inhibit fibroblast swarms from developing, such as GAP 27, could lead to new therapeutics for preventing or reducing scar formation in human wounds.

Based on our findings, we propose a new model of mammalian scarring involving selective gap junction expression and cell-cell communication needed for fibroblast

swarming towards formative scar centres (**Fig. 5.1**). The recruitment of scar-competent fibroblasts from outside wounds has enormous clinical significance. Strategies that inhibit fibroblast swarms from developing, such as GAP 27, could lead to new therapeutics for preventing or reducing scar formation in human wounds.

We believe that fibroblast swarming and matrix movements are likely a universal wound response to injuries in mammalian tissues and organs and not restricted to back skin. Support to this tenet comes from functional experiments on kidney and lung fibrosis. Study proved that calcium fluid inhibition in fibroblasts release bleomycin-induced pulmonary fibrosis in mice and high-level Ca^{2+} trigger Cx hemichannel opening (De Vuyst et al., 2006; Mukherjee et al., 2015). Here, we observe that gap junctions coordinate the collective swarms of scar-competent fascia fibroblasts and matrix into wounds and not by their association with the granulation tissue as was previously proposed. Therefore, fibroblast/matrix aggregations within the injured internal organs may thus contribute to scarring in the same way as shown here in skin.

The study in thesis suggests that therapeutic blockade of Cx43 on human patient wounds alters collective behaviours of scar-forming fibroblasts, abrogates the movement of the subcutaneous fascia, and results in reduced scarring. The described molecular mechanism underlying anti-fibrotic effect of Cx43 inhibition adds a piece of strong evidence that targeting Cx43 or Ca^{2+} signalling represents novel therapeutic strategies to curtail fibrosis and scarring.
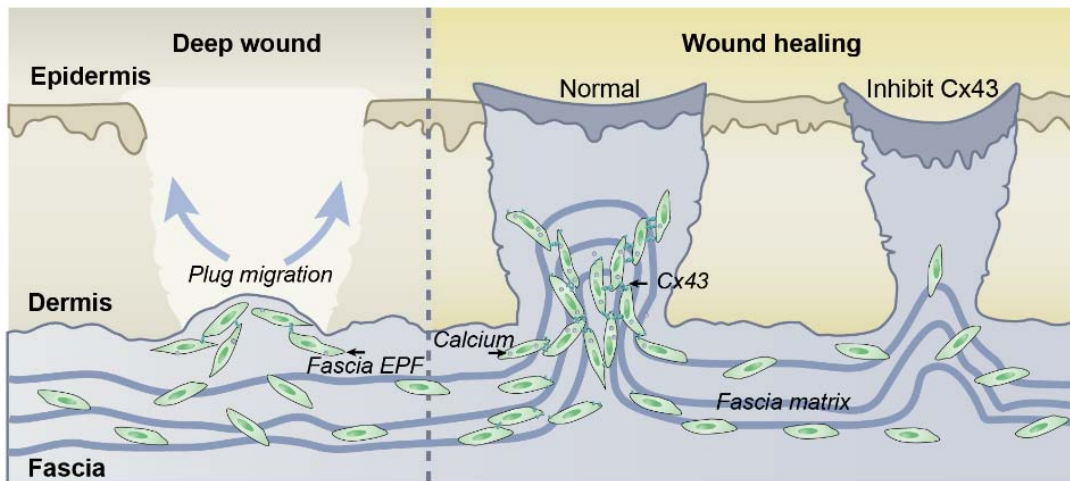
Figure 8.1   Mechanism of wound repair by Cx43. During wound healing, EPFs in fascia migrate collectively, swarming towards wound centre, and trigger surrounding fascia matrix flocking into wounds. Cx43 inhibition attenuates scar formation by disrupting calcium oscillations in EPFs and subsequent inhibition of EPFs swarming and fascia matrix movement. Gap junction-mediated inter-EPF communication plays a key role in matrix outpouring and scar formation, and necessary for patch repair of voluminous wounds.

Abbreviations

Abbreviation	Definition
2-APB	2-Aminoethoxydiphenyl borate
3D	Three Dimensional
AF488	Alexa Fluor 488
ANOVA	Analysis of Variance
ATP	Adenosine triphosphate
BF	Bright field
BSA	Bovine serum albumin
Ca2+	Calcium ions
Calcein-AM	calcein acetoxymethyl
cAMP	Cyclic adenosine monophosphate
CDH2	Cadherin 2
CO2	Carbon dioxide
Col1	Collagen type I
Col3	Collagen type III
Cx43	Connexin 43
DETCs	dendritic epidermal T cells
DMEM	Dulbecco's modified Eagle's Medium
DMSO	Dimethyl sulfoxide
dNTPs	Deoxynucleoside triphosphates
ECM	extracellular matrix

Abbreviation	Definition
En1	Engrailed-1
ENFs	En1-lineage-naive fibroblasts
EPFs	En1-lineage-positive fibroblasts
FACs	Fluorescence-activated cell sorting
FBS	Fetal bovine serum
FITC	Fluorescein isothiocyanate
HBSS	Hank's Balanced Salt Solution
IC50	Half maximal inhibitory concentration
IL-10	Interleukin 10
IL-23	Interleukin 23
IL-24	Interleukin 24
IL-6	Interleukin 6
IL-8	Interleukin 8
ILCs	Innate lymphoid cells
min	Minute
mL	Milliliter
mm	Millimeter
MMF	Medetomidine, midazolam and fentanyl mixture
MMPs	Metalloproteinases
Na^+	Sodium ions
OCT	Optimal cutting temperature compound

Abbreviation	Definition
ODDD	oculodentodigital dysplasia
P120ctn/ Rho	120 catenin/ Rho family GTPase
PBS	Phosphate-buffered saline
PCR	Polymerase chain reaction
PFA	paraformaldehyde
SC	Stratum corneum
SCID	Severe combined immunodeficient mice
SEM	standard error of mean
TAE	Tris-acetate-EDTA
TGF-β	Transforming growth factor-beta
TIMPs	inhibitors of metalloproteinases
TNF-α	Tumor necrosis factor-a
UV	Ultraviolet light
VEGF	Vascular endothelial growth factor
WNFs	Wnt-lineage-naive fibroblasts
WPFs	Wnt-lineage-positive fibroblasts
ZO-1	Zonula occludens-1
µM	micromole per liter

Reference

Bayat, A., D.A. McGrouther, and M.W. Ferguson. 2003. Skin scarring. *BMJ* 326:88-92.

Becker, D.L., C. Thrasivoulou, and A.R. Phillips. 2012. Connexins in wound healing; perspectives in diabetic patients. *Biochim Biophys Acta* 1818:2068-2075.

Bennett, B.C., M.D. Purdy, K.A. Baker, C. Acharya, W.E. McIntire, R.C. Stevens, Q. Zhang, A.L. Harris, R. Abagyan, and M. Yeager. 2016. An electrostatic mechanism for Ca(2+)-mediated regulation of gap junction channels. *Nat Commun* 7:8770.

Benninger, R.K., M. Zhang, W.S. Head, L.S. Satin, and D.W. Piston. 2008. Gap junction coupling and calcium waves in the pancreatic islet. *Biophys J* 95:5048-5061.

Brodskiy, P.A., and J.J. Zartman. 2018. Calcium as a signal integrator in developing epithelial tissues. *Phys Biol* 15:051001.

Chen, F.M., and X. Liu. 2016. Advancing biomaterials of human origin for tissue engineering. *Prog Polym Sci* 53:86-168.

Chen, Q., A. Boire, X. Jin, M. Valiente, E.E. Er, A. Lopez-Soto, L. Jacob, R. Patwa, H. Shah, K. Xu, J.R. Cross, and J. Massague. 2016. Carcinoma-astrocyte gap junctions promote brain metastasis by cGAMP transfer. *Nature* 533:493-498.

Coentro, J.Q., E. Pugliese, G. Hanley, M. Raghunath, and D.I. Zeugolis. 2018. Current and upcoming therapies to modulate skin scarring and fibrosis. *Adv Drug Deliv Rev*

Cogliati, B., M. Vinken, T.C. Silva, C.M.M. Araujo, T.P.A. Aloia, L.M. Chaible, C.M.C. Mori, and M.L.Z. Dagli. 2015. Connexin 43 deficiency accelerates skin wound healing and extracellular matrix remodeling in mice. *J Dermatol Sci* 79:50-56.

Coles, M.C., and C.D. Buckley. 2019. Ready-made cellular plugs heal skin wounds. *Nature* 576:215-216.

Correa-Gallegos, D., D. Jiang, S. Christ, P. Ramesh, H. Ye, J. Wannemacher, S. Kalgudde Gopal, Q. Yu, M. Aichler, A. Walch, U. Mirastschijski, T. Volz, and Y. Rinkevich. 2019. Patch repair of deep wounds by mobilized fascia. *Nature* 576:287-292.

Cotrina, M.L. 1998. connexins regulate calcium signaling by controlling ATP release *PNAS* Vol. 95, pp. 15735–15740:

De Vuyst, E., E. Decrock, L. Cabooter, G.R. Dubyak, C.C. Naus, W.H. Evans, and L. Leybaert. 2006. Intracellular calcium changes trigger connexin 32 hemichannel opening. *EMBO J* 25:34-44.

Derangeon, M., N. Bourmeyster, I. Plaisance, C. Pinet-Charvet, Q. Chen, F. Duthe, M.R. Popoff, D. Sarrouilhe, and J.C. Herve. 2008. RhoA GTPase and F-actin

dynamically regulate the permeability of Cx43-made channels in rat cardiac myocytes. *J Biol Chem* 283:30754-30765.

Dorsett-Martin, W.A. 2004. Rat models of skin wound healing: a review. *Wound Repair Regen* 12:591-599.

Dovi, J.V., A.M. Szpaderska, and L.A. DiPietro. 2004. Neutrophil function in the healing wound: adding insult to injury? *Thromb Haemost* 92:275-280.

Driskell, R.R., B.M. Lichtenberger, E. Hoste, K. Kretzschmar, B.D. Simons, M. Charalambous, S.R. Ferron, Y. Herault, G. Pavlovic, A.C. Ferguson-Smith, and F.M. Watt. 2013. Distinct fibroblast lineages determine dermal architecture in skin development and repair. *Nature* 504:277-281.

Elbadawy, H.M., P. Mirabelli, M. Xeroudaki, M. Parekh, M. Bertolin, C. Breda, C. Cagini, D. Ponzin, N. Lagali, and S. Ferrari. 2016. Effect of connexin 43 inhibition by the mimetic peptide Gap27 on corneal wound healing, inflammation and neovascularization. *Br J Pharmacol* 173:2880-2893.

Epstein, E.H., Jr., and N.H. Munderloh. 1978. Human skin collagen. Presence of type I and type III at all levels of the dermis. *J Biol Chem* 253:1336-1337.

Evans, W.H., and L. Leybaert. 2007. Mimetic peptides as blockers of connexin channel-facilitated intercellular communication. *Cell Commun Adhes* 14:265-273.

Francis, R., X. Xu, H. Park, C.J. Wei, S. Chang, B. Chatterjee, and C. Lo. 2011. Connexin43 modulates cell polarity and directional cell migration by regulating microtubule dynamics. *PLoS One* 6:e26379.

Friedl, P., Y. Hegerfeldt, and M. Tusch. 2004. Collective cell migration in morphogenesis and cancer. *Int J Dev Biol* 48:441-449.

Friedl, P., J. Locker, E. Sahai, and J.E. Segall. 2012. Classifying collective cancer cell invasion. *Nat Cell Biol* 14:777-783.

Fujimori, T., A. Nakajima, N. Shimada, and S. Sawai. 2019. Tissue self-organization based on collective cell migration by contact activation of locomotion and chemotaxis. *Proc Natl Acad Sci U S A* 116:4291-4296.

Gabbiani, G. 1998. Evolution and clinical implications of the myofibroblast concept. *Cardiovascular Research* 38:545-548.

Gauglitz, G.G., H.C. Korting, T. Pavicic, T. Ruzicka, and M.G. Jeschke. 2011. Hypertrophic scarring and keloids: pathomechanisms and current and emerging treatment strategies. *Mol Med* 17:113-125.

Glass, B.J., R.G. Hu, A.R. Phillips, and D.L. Becker. 2015. The action of mimetic peptides on connexins protects fibroblasts from the negative effects of ischemia reperfusion. *Biol Open* 4:1473-1480.

Govindarajan, R., S. Chakraborty, K.E. Johnson, M.M. Falk, M.J. Wheelock, K.R. Johnson, and P.P. Mehta. 2010. Assembly of connexin43 into gap junctions is regulated differentially by E-cadherin and N-cadherin in rat liver epithelial cells. *Mol Biol Cell* 21:4089-4107.

Gurtner, G.C., S. Werner, Y. Barrandon, and M.T. Longaker. 2008. Wound repair and regeneration. *Nature* 453:314-321.

Harris, A.L. 2001. Emerging issues of connexin channels: biophysics fills the gap. *Q Rev Biophys* 34:325-472.

Hinz, B. 2016. The role of myofibroblasts in wound healing. *Curr Res Transl Med* 64:171-177.

Hinz, B., S.H. Phan, V.J. Thannickal, A. Galli, M.L. Bochaton-Piallat, and G. Gabbiani. 2007. The myofibroblast: one function, multiple origins. *Am J Pathol* 170:1807-1816.

Huang, R.P., Y. Fan, M.Z. Hossain, A. Peng, Z.L. Zeng, and A.L. Boynton. 1998. Reversion of the neoplastic phenotype of human glioblastoma cells by connexin 43 (cx43). *Cancer Res* 58:5089-5096.

Inman, G.J., F.J. Nicolas, J.F. Callahan, J.D. Harling, L.M. Gaster, A.D. Reith, N.J. Laping, and C.S. Hill. 2002. SB-431542 is a potent and specific inhibitor of transforming growth factor-beta superfamily type I activin receptor-like kinase (ALK) receptors ALK4, ALK5, and ALK7. *Mol Pharmacol* 62:65-74.

Jiang, D., D. Correa-Gallegos, S. Christ, A. Stefanska, J. Liu, P. Ramesh, V. Rajendran, M.M. De Santis, D.E. Wagner, and Y. Rinkevich. 2018. Two succeeding fibroblastic lineages drive dermal development and the transition from regeneration to scarring. *Nat Cell Biol* 20:422-431.

Jiang, D., K. Singh, J. Muschhammer, S. Schatz, A. Sindrilaru, E. Makrantonaki, Y. Qi, M. Wlaschek, and K. Scharffetter-Kochanek. 2020. MSCs rescue impaired wound healing in a murine LAD1 model by adaptive responses to low TGF-beta1 levels. *EMBO Rep* e49115.

Kanitakis, J. 2002. Anatomy, histology and immunohistochemistry of normal human skin. *Eur J Dermatol* 12:390-399; quiz 400-391.

Karppinen, S.M., R. Heljasvaara, D. Gullberg, K. Tasanen, and T. Pihlajaniemi. 2019. Toward understanding scarless skin wound healing and pathological scarring. *F1000Res* 8:

Kiang, D.T., R. Kollander, H.H. Lin, S. LaVilla, and M.M. Atkinson. 1994. Measurement of gap junctional communication by fluorescence activated cell sorting. *In Vitro Cell Dev Biol Anim* 30A:796-802.

Kim, M.H., W. Liu, D.L. Borjesson, F.R. Curry, L.S. Miller, A.L. Cheung, F.T. Liu, R.R. Isseroff, and S.I. Simon. 2008. Dynamics of neutrophil infiltration during

cutaneous wound healing and infection using fluorescence imaging. *J Invest Dermatol* 128:1812-1820.

Kotini, M., E.H. Barriga, J. Leslie, M. Gentzel, V. Rauschenberger, A. Schambony, and R. Mayor. 2018. Gap junction protein Connexin-43 is a direct transcriptional regulator of N-cadherin *in vivo*. *Nat Commun* 9:3846.

Krutovskikh, V., and H. Yamasaki. 2000. Connexin gene mutations in human genetic diseases. *Mutation Research/Reviews in Mutation Research* 462:197-207.

Kurpios, N.A., M. Ibanes, N.M. Davis, W. Lui, T. Katz, J.F. Martin, J.C. Izpisua Belmonte, and C.J. Tabin. 2008. The direction of gut looping is established by changes in the extracellular matrix and in cell:cell adhesion. *Proc Natl Acad Sci U S A* 105:8499-8506.

Larson, B.J., M.T. Longaker, and H.P. Lorenz. 2010. Scarless fetal wound healing: a basic science review. *Plast Reconstr Surg* 126:1172-1180.

Lee, J., R. Böscke, P.-C. Tang, B.H. Hartman, S. Heller, and K.R. Koehler. 2018. Hair Follicle Development in Mouse Pluripotent Stem Cell-Derived Skin Organoids. *Cell Reports* 22:242-254.

Lee, S.H., S.K. Jeong, and S.K. Ahn. 2006. An update of the defensive barrier function of skin. *Yonsei Med J* 47:293-306.

Lembong, J., B. Sabass, and H.A. Stone. 2017. Calcium oscillations in wounded fibroblast monolayers are spatially regulated through substrate mechanics. *Phys Biol* 14:045006.

Li, A., J.H. Cho, B. Reid, C.C. Tseng, L. He, P. Tan, C.Y. Yeh, P. Wu, Y. Li, R.B. Widelitz, Y. Zhou, M. Zhao, R.H. Chow, and C.M. Chuong. 2018. Calcium oscillations coordinate feather mesenchymal cell movement by SHH dependent modulation of gap junction networks. *Nat Commun* 9:5377.

Li, X., L. Guo, X. Yang, J. Wang, Y. Hou, S. Zhu, J. Du, J. Feng, Y. Xie, L. Zhuang, X. He, and Y. Liu. 2019. TGF-beta1-Induced Connexin43 Promotes Scar Formation via the Erk/MMP-1/Collagen III Pathway. *J Oral Rehabil*

Lin, J.H.C., J. Yang, S. Liu, T. Takano, X. Wang, Q. Gao, K. Willecke, and M. Nedergaard. 2003. Connexin Mediates Gap Junction-Independent Resistance to Cellular Injury. *The Journal of Neuroscience* 23:430-441.

Lynch, M.D., and F.M. Watt. 2018. Fibroblast heterogeneity: implications for human disease. *J Clin Invest* 128:26-35.

Marshall, C.D., M.S. Hu, T. Leavitt, L.A. Barnes, H.P. Lorenz, and M.T. Longaker. 2018. Cutaneous Scarring: Basic Science, Current Treatments, and Future Directions. *Adv Wound Care (New Rochelle)* 7:29-45.

Matsuuchi, L., and C.C. Naus. 2013. Gap junction proteins on the move: connexins, the cytoskeleton and migration. *Biochim Biophys Acta* 1828:94-108.

McNeil, P.L., and R.A. Steinhardt. 2003. Plasma membrane disruption: repair, prevention, adaptation. *Annu Rev Cell Dev Biol* 19:697-731.

Michon, L., R. Nlend Nlend, S. Bavamian, L. Bischoff, N. Boucard, D. Caille, J. Cancela, A. Charollais, E. Charpantier, P. Klee, M. Peyrou, C. Populaire, L. Zulianello, and P. Meda. 2005. Involvement of gap junctional communication in secretion. *Biochim Biophys Acta* 1719:82-101.

Moll, I., M. Roessler, J.M. Brandner, A.C. Eispert, P. Houdek, and R. Moll. 2005. Human Merkel cells--aspects of cell biology, distribution and functions. *Eur J Cell Biol* 84:259-271.

Montgomery, J., G.S. Ghatnekar, C.L. Grek, K.E. Moyer, and R.G. Gourdie. 2018. Connexin 43-Based Therapeutics for Dermal Wound Healing. *Int J Mol Sci* 19:

Mori, R., K.T. Power, C.M. Wang, P. Martin, and D.L. Becker. 2006. Acute downregulation of connexin43 at wound sites leads to a reduced inflammatory response, enhanced keratinocyte proliferation and wound fibroblast migration. *J Cell Sci* 119:5193-5203.

Mukherjee, S., E.A. Ayaub, J. Murphy, C. Lu, M. Kolb, K. Ask, and L.J. Janssen. 2015. Disruption of Calcium Signaling in Fibroblasts and Attenuation of Bleomycin-Induced Fibrosis by Nifedipine. *Am J Respir Cell Mol Biol* 53:450-458.

Mukherjee, S., F. Duan, M.R. Kolb, and L.J. Janssen. 2013. Platelet derived growth factor-evoked Ca2+ wave and matrix gene expression through phospholipase C in human pulmonary fibroblast. *Int J Biochem Cell Biol* 45:1516-1524.

Muller-Rover, S., B. Handjiski, C. van der Veen, S. Eichmuller, K. Foitzik, I.A. McKay, K.S. Stenn, and R. Paus. 2001. A comprehensive guide for the accurate classification of murine hair follicles in distinct hair cycle stages. *J Invest Dermatol* 117:3-15.

Nakano, Y., M. Oyamada, P. Dai, T. Nakagami, S. Kinoshita, and T. Takamatsu. 2008. Connexin43 knockdown accelerates wound healing but inhibits mesenchymal transition after corneal endothelial injury *in vivo*. *Invest Ophthalmol Vis Sci* 49:93-104.

Nielsen, M.S., L.N. Axelsen, P.L. Sorgen, V. Verma, M. Delmar, and N.H. Holstein-Rathlou. 2012. Gap junctions. *Compr Physiol* 2:1981-2035.

Nishiguchi, M.A., C.A. Spencer, D.H. Leung, and T.H. Leung. 2018. Aging Suppresses Skin-Derived Circulating SDF1 to Promote Full-Thickness Tissue Regeneration. *Cell Rep* 24:3383-3392 e3385.

Ogawa, R. 2017. Keloid and Hypertrophic Scars Are the Result of Chronic Inflammation in the Reticular Dermis. *Int J Mol Sci* 18:

Oyamada, M., Y. Oyamada, and T. Takamatsu. 2005. Regulation of connexin expression. *Biochim Biophys Acta* 1719:6-23.

Pasparakis, M., I. Haase, and F.O. Nestle. 2014. Mechanisms regulating skin immunity and inflammation. *Nat Rev Immunol* 14:289-301.

Patel, S.J., J.M. Milwid, K.R. King, S. Bohr, A. Iracheta-Vellve, M. Li, A. Vitalo, B. Parekkadan, R. Jindal, and M.L. Yarmush. 2012. Gap junction inhibition prevents drug-induced liver toxicity and fulminant hepatic failure. *Nat Biotechnol* 30:179-183.

Pearson, R.A., N.L. Luneborg, D.L. Becker, and P. Mobbs. 2005. Gap junctions modulate interkinetic nuclear movement in retinal progenitor cells. *J Neurosci* 25:10803-10814.

Qiu, C., P. Coutinho, S. Frank, S. Franke, L.Y. Law, P. Martin, C.R. Green, and D.L. Becker. 2003. Targeting connexin43 expression accelerates the rate of wound repair. *Curr Biol* 13:1697-1703.

Rinkevich, Y., G.G. Walmsley, M.S. Hu, Z.N. Maan, A.M. Newman, M. Drukker, M. Januszyk, G.W. Krampitz, G.C. Gurtner, H.P. Lorenz, I.L. Weissman, and M.T. Longaker. 2015. Skin fibrosis. Identification and isolation of a dermal lineage with intrinsic fibrogenic potential. *Science* 348:aaa2151.

Saidi Brikci-Nigassa, A., M.J. Clement, T. Ha-Duong, E. Adjadj, L. Ziani, D. Pastre, P.A. Curmi, and P. Savarin. 2012. Phosphorylation controls the interaction of the connexin43 C-terminal domain with tubulin and microtubules. *Biochemistry* 51:4331-4342.

Shaw, T.J., and P. Martin. 2009. Wound repair at a glance. *J Cell Sci* 122:3209-3213.

Sorgen, P.L., H.S. Duffy, P. Sahoo, W. Coombs, M. Delmar, and D.C. Spray. 2004. Structural Changes in the Carboxyl Terminus of the Gap Junction Protein Connexin43 Indicates Signaling between Binding Domains for c-Src and Zonula Occludens-1. *Journal of Biological Chemistry* 279:54695-54701.

Sougrat, R., M. Morand, C. Gondran, P. Barre, R. Gobin, F. Bonte, M. Dumas, and J.M. Verbavatz. 2002. Functional expression of AQP3 in human skin epidermis and reconstructed epidermis. *J Invest Dermatol* 118:678-685.

Stappenbeck, T.S., and H. Miyoshi. 2009. The role of stromal stem cells in tissue regeneration and wound repair. *Science* 324:1666-1669.

Tarzemany, R., G. Jiang, J.X. Jiang, H. Larjava, and L. Hakkinen. 2017. Connexin 43 Hemichannels Regulate the Expression of Wound Healing-Associated Genes in Human Gingival Fibroblasts. *Sci Rep* 7:14157.

toshihiko. 1998. Intercellular Calcium Signaling via Gap Junction in Connexin-43-transfected Cells.

Tseng Q, D.-P.E., Deshiere A, Balland M, Guillou H, Filhol O, Théry M. 2012. Spatial organization of the extracellular matrix regulates cell-cell junction positioning. *Proc Natl Acad Sci U S A.* 109(5):1506-1511.

Unger, V.M., N.M. Kumar, N.B. Gilula, and M. Yeager. 1999. Three-dimensional structure of a recombinant gap junction membrane channel. *Science* 283:1176-1180.

Watts, G.T. 1960. Wound shape and tissue tension in healing. *Br J Surg* 47:555-561.

Wickett, R.R., and M.O. Visscher. 2006. Structure and function of the epidermal barrier. *American Journal of Infection Control* 34:S98-S110.

Wong, P., T. Tan, C. Chan, V. Laxton, Y.W. Chan, T. Liu, W.T. Wong, and G. Tse. 2016. The Role of Connexins in Wound Healing and Repair: Novel Therapeutic Approaches. *Front Physiol* 7:596.

Wong, V.W., M. Sorkin, J.P. Glotzbach, M.T. Longaker, and G.C. Gurtner. 2011. Surgical approaches to create murine models of human wound healing. *J Biomed Biotechnol* 2011:969618.

Wright, C.S., M.A.M. van Steensel, M.B. Hodgins, and P.E.M. Martin. 2009. Connexin mimetic peptides improve cell migration rates of human epidermal keratinocytes and dermal fibroblasts in vitro. *Wound Repair and Regeneration* 17:240-249.

Wright, J.A., T. Richards, and D.L. Becker. 2012. Connexins and diabetes. *Cardiol Res Pract* 2012:496904.

Wynn, T.A. 2008. Cellular and molecular mechanisms of fibrosis. *J Pathol* 214:199-210.

Yang, Y., M.H. Cao, Q. Wang, D.D. Yuan, L. Li, and L. Tao. 2011. The effects of 2-aminoethoxydiphenyl borate and diphenylboronic anhydride on gap junctions composed of Connexin43 in TM(4) sertoli cells. *Biol Pharm Bull* 34:1390-1397.

Yun, S.M., S.H. Kim, and E.H. Kim. 2019. The Molecular Mechanism of Transforming Growth Factor-beta Signaling for Intestinal Fibrosis: A Mini-Review. *Front Pharmacol* 10:162.

Zhang, X.F., and X. Cui. 2017. Connexin 43: Key roles in the skin. *Biomed Rep* 6:605-611.

Zhou, J.Z., and J.X. Jiang. 2014. Gap junction and hemichannel-independent actions of connexins on cell and tissue functions--an update. *FEBS Lett* 588:1186-1192.

Publications

Connexin43 gap junction drives fascia mobilization and repair of deep skin wounds.

Wan L, Jiang D., Correa-Gallegos D., Ramesh P., Zhao J., Ye H, et al.

Matrix Biol. 2021;97:58-71.

Injury triggers fascia fibroblast collective cell migration to drive scar formation through N-cadherin

Jiang D., Christ S., Correa-Gallegos D., Ramesh P., Kalgudde Gopal S., Wannemacher J., Mayr C.H., Lupperger V., Yu Q., Ye H., Muck-Hausl M., Rajendran V., **Wan L.,** Liu J., Mirastschijski U., Volz T., Marr C., Schiller H.B., and Rinkevich Y..

Nat Commun. 2020;11:5653.

Affidavit

Affidavit

I hereby declare, that the submitted thesis entitled:

Connexin43 gap junction drives fascia matrix mobilization and repair of deep skin wounds
………………………………………………………………………………………………….

is my own work. I have only used the sources indicated and have not made unauthorized use of services of a third party. Where the work of others has been quoted or reproduced, the source is always given.

I further declare that the submitted thesis or parts thereof have not been presented as part of an examination degree to any other university.

Munich, 08.07.2021   Li WAN
place, date   Signature doctoral candidate

Acknowledgment

It is hard to come here, I just realized that time is going away without waiting for anybody. Until I finished the final part, thanksgiving just emerged in my mind that many people encouraged me, helped me and even pushed me through my doctoral study. To be here, I would like to and have to express my sincere appreciation to all of the people.

First, I am thanking my supervisor, Professor Dr. med. Jürgen Behr, the most kindly master in Medizinische Klinik und Poliklinik V at the Ludwigs-Maximilian University of Munich in Germany. It is he who accepted me as one doctoral student in Human Biology (Dr. rer. biol. hum.). Under his kind supervision together with help from co-supervisor, Dr. Yuval Rinkevich, the youngest scientist in Helmholtz Institute, I conducted my doctoral study. They devoted great effort and endless energy to this prestigious international research institute.

I thank all colleagues in our lab, especially Ms. Sandra Schiener, secretary of Dr. Rinkevich, and Dr. Juliane Wannemacher, laboratory Manager. Those excellent people are always kind to help me no matter whether in my work or in my life. In addition, I thank my dear lab colleague, Dr. Dongsheng Jiang, who helped me a lot in this project and paper revising, and Mr. Donovon Correa Gallegos, Mr. Haifeng Ye, Mr. Pushkar Ramesh, Mr. Jiakuan Zhao in favor of me performing some experiments. With my great thanks to all the other members in our lab and Institute, I would say, "Thank you!"

Most importantly, I cannot refuse to thank the Chinese Scholarship Council & LMU Grant. They accepted me as a doctoral candidate and financed me to focus on study.

Their generosity inspired me to help others and give back to the community. I hope one day that I will contribute to help others to achieve their goals.

Finally, my deepest profound gratitude should be given to my family, my parents and my husband for providing me unfailing support. They help me release pressure and accompany me through lots of good and bad times in my study and daily life. The accomplishment would not be achieved without them.